

Unified field theoretical approach to deep and recurrent neuronal networks

Kai Segadlo^{1,2,*}, Bastian Epping^{2,3,*}, Alexander van Meegen^{2,4,*}, David Dahmen², Michael Krämer³ and Moritz Helias^{1,2}

¹ Department of Physics, Faculty 1, RWTH Aachen University, Aachen, Germany

² Institute of Neuroscience and Medicine (INM-6) and Institute for Advanced Simulation (IAS-6) and JARA-Institute Brain Structure-Function Relationships (INM-10), Jülich Research Centre, Jülich, Germany

³ Institute for Theoretical Particle Physics and Cosmology, RWTH Aachen University, Aachen, Germany

⁴ Institute of Zoology, University of Cologne, Cologne, Germany

* Equal contribution

Abstract. Understanding capabilities and limitations of different network architectures is of fundamental importance to machine learning. Bayesian inference on Gaussian processes has proven to be a viable approach for studying recurrent and deep networks in the limit of infinite layer width, $n \rightarrow \infty$. Here we present a unified and systematic derivation of the mean-field theory for both architectures that starts from first principles by employing established methods from statistical physics of disordered systems. The theory elucidates that while the mean-field equations are different with regard to their temporal structure, they yet yield identical Gaussian kernels when readouts are taken at a single time point or layer, respectively. Bayesian inference applied to classification then predicts identical performance and capabilities for the two architectures. Numerically, we find that convergence towards the mean-field theory is typically slower for recurrent networks than for deep networks and the convergence speed depends non-trivially on the parameters of the weight prior as well as the depth or number of time steps, respectively. Our method exposes that Gaussian processes are but the lowest order of a systematic expansion in $1/n$ and we compute next-to-leading-order corrections which turn out to be architecture-specific. The formalism thus paves the way to investigate the fundamental differences between recurrent and deep architectures at finite widths n .

Contents

1	Introduction	2
2	Theoretical background	4
2.1	Bayesian supervised learning	4
2.2	Network architectures	5
2.3	Parameter priors	6
3	Unified field theoretical approach to RNNs and DNNs	6
3.1	Marginalization of the parameter prior	7
3.2	Auxiliary variables	8
3.3	Saddle-point approximation	9
3.4	Network prior	10
3.5	Predictive distribution	10
4	Comparison of RNNs and DNNs	11
4.1	Kernel	12
4.2	Predictive distribution	13
4.3	Next-to-leading order corrections	14
5	Discussion	18
6	Appendix	21
6.1	Unified field theoretical approach for multiple input sequences	21
6.1.1	Action and auxiliary variables	21
6.1.2	Saddle-point approximation	26
6.2	Finite-size instability of RNNs	26
6.3	Mean-field theory for error function nonlinearity	27
6.4	Details about numerical experiments	28
6.5	Next-to-leading-order corrections	29
6.5.1	DNN	30
6.5.2	RNN	32

1. Introduction

Deep learning has brought a dramatic improvement of the state-of-the-art in many fields of data science, ranging from speech recognition and translation to visual object classification [1–4]. Any progress in the empirically-driven improvement of algorithms must be accompanied by a profound understanding of why and how deep learning works. Such an understanding is needed to provide guarantees, for example about the accuracy and the robustness of the networks, and will help preventing the frequently reported failures of deep learning, such as its vulnerability to adversarial examples [5].

A common method to obtain analytical insight into deep networks is to study the overparametrized limit in which the width n_ℓ of all layers ℓ tends to infinity. In this limit, it has been shown with the help of the multivariate central limit theorem that under a Gaussian prior on the weights $W^{(\ell)}$ in each layer, the pre-activations follow a Gaussian process with an iteratively determined covariance [6–9]; in particular, the pre-activations across different layers and across different neurons become independently Gaussian distributed. This approach allows one to investigate

learning and prediction in the framework of Bayesian inference [7]. There is a prominent orthogonal line of work based on the neural tangent kernel [10] which investigates gradient-based learning in the large n_ℓ limit; in this manuscript, we exclusively focus on Bayesian inference (in this context often called NNGP; see [11] for an empirical performance comparison of the two approaches).

Often, analogies are drawn between deep neural networks (DNNs) and discrete-time recurrent neural networks (RNNs): Unrolling time in RNNs formally converts them to DNNs, however with shared weights $W^{(\ell)} \equiv W \forall \ell$ across layers of identical size $n_\ell \equiv n \forall \ell$. This led to parallel developments in terms of training strategies for both architectures, such as backpropagation [12] and backpropagation through time [13].

There are, however, a number of open issues when applying mean-field theory to deep and recurrent neural networks. First of all, the approximation as a Gaussian process relies on the central limit theorem and is thus strictly valid only in the limit of infinite layer widths $n_\ell \rightarrow \infty$. Moreover, due to weight sharing, pre-activations for different points in time are not statistically independent in RNNs; the central limit theorem is thus not applicable and the mean-field approximation becomes uncontrolled. Several studies still find that the mean-field theories of DNNs and RNNs appear to be closely related, culminating in ref. [14] which formulates a variety of network architectures as tensor programs and finds that most common network architectures, under certain conditions on the nonlinearities and priors, converge in distribution to a Gaussian process (see also [15, 16] for an extension of the neural tangent kernel to recurrent networks). But the relationship between the Gaussian processes for RNNs and DNNs has so far not been addressed.

The agreement of the mean-field predictions with the performance of finite-size networks is based on numerical evidence so far. Furthermore, in the limit of infinite width the number of trainable parameters of a DNN, $\sum_{\ell=1}^L n_{\ell+1} n_\ell \rightarrow \infty$, and of an RNN, $n^2 \rightarrow \infty$, both tend to infinity and do not enter explicitly in the result of the Gaussian approximation. The Gaussian process thus has limited capability of quantifying the expressivity of neural networks in relation to the required resources, such as the number of trained weights. Studies on finite-size corrections beyond the $n_\ell \rightarrow \infty$ limit are so far restricted to DNNs [17–28] (but see [29] for stationary continuous-time recurrent networks). Understanding the limits of the putative equivalence of DNNs and RNNs on the mean-field level requires a common theoretical basis for the two architectures that would extend to finite n and finite n_ℓ .

To overcome these limitations, we here combine the established view of Bayesian inference by Gaussian processes [30] with statistical field theory applied to neural networks [31–36]. These methods have been developed in the field of disordered systems, which are systems with random parameters, such as spin glasses [37–39] and are able to extract the typical behavior of a system with a large number of interacting components. For example, this approach has recently been used to characterize the typical richness, represented by the entropy, of Boolean functions computed in the output layer of DNNs, RNNs, and sparse Boolean circuits [40].

Concretely, in this paper, we present a systematic derivation of the mean-field theories for DNNs and RNNs that is based on the well-established approach of field theory for recurrent networks [31, 35, 41, 42], which allows a unified treatment of the two architectures [40]. This paves the way for extensions to finite n, n_ℓ , enabled by a rich set of systematic methods available in the mathematical physics literature to compute corrections beyond the leading order [43, 44]. Already to leading order,

we find that the mean-field theories of DNNs and RNNs are in fact qualitatively different with regard to correlations across layers or time, respectively. The predictive distribution in Bayesian training is therefore in general different between the two architectures. Nonetheless, the structure of the mean-field equations can give rise to the same Gaussian processes kernel in the limit of infinite width for both DNNs and RNNs if the readout in the RNN is taken from a single time step. This finding holds for single inputs, as pointed out in ref. [40], as well as input sequences. Furthermore, for a point-symmetric activation function [40], there is no observable difference between DNNs and RNNs on the mean-field level if the biases are uncorrelated in time and the input is only supplied in the first time step. Going beyond the leading order, we compute the next-to-leading-order corrections for both DNNs and RNNs. These corrections reveal commonalities and differences between the architectures: In both architectures external fluctuations from the input are transmitted by the same linear response function to the readout layer or time-point. This response decays exponentially, with identical decay constant with depth or time, respectively. At the transition to chaos this decay constant diverges. The intrinsically generated finite-size fluctuations, however, differ with respect to their layer wise or temporal statistics, respectively. In particular, cross-time fluctuations drive fluctuations in RNNs overall to a higher level than in DNNs, where only equal-layer fluctuations drive fluctuations.

2. Theoretical background

2.1. Bayesian supervised learning

First, we briefly review the Bayesian approach to supervised learning [45]. Let $p(\mathbf{y} | \mathbf{x}, \boldsymbol{\theta})$ be a model (here DNN or RNN) that maps inputs $\mathbf{x} \in \mathbb{R}^{n_{\text{in}}}$ to outputs $\mathbf{y} \in \mathbb{R}^{n_{\text{out}}}$ and that depends on a set of parameters $\boldsymbol{\theta}$. Conventional training of such a model corresponds to finding a particular parameter set $\hat{\boldsymbol{\theta}}$ that maximizes the likelihood $p(\mathbf{Y} | \mathbf{X}, \boldsymbol{\theta})$ for some given training data $\mathbf{D} = \{\mathbf{X}, \mathbf{Y}\}$, with $\mathbf{X} \in \mathbb{R}^{n_D \times n_{\text{in}}}$ and $\mathbf{Y} \in \mathbb{R}^{n_D \times n_{\text{out}}}$. A prediction for the output \mathbf{y}^* caused by an unseen test input \mathbf{x}^* is then given by $p(\mathbf{y}^* | \mathbf{x}^*, \hat{\boldsymbol{\theta}})$. In the Bayesian view, one instead assumes a prior distribution of parameters $p(\boldsymbol{\theta})$ to obtain, via Bayes' rule, an entire posterior distribution of the parameters

$$p(\boldsymbol{\theta} | \mathbf{Y}, \mathbf{X}) = \frac{p(\mathbf{Y} | \mathbf{X}, \boldsymbol{\theta}) p(\boldsymbol{\theta})}{\int d\boldsymbol{\theta} p(\mathbf{Y} | \mathbf{X}, \boldsymbol{\theta}) p(\boldsymbol{\theta})}. \quad (1)$$

The conditioning on the training data in $p(\boldsymbol{\theta} | \mathbf{Y}, \mathbf{X})$ can be interpreted as selecting, among all possible parameter sets given by the prior $p(\boldsymbol{\theta})$, those parameter sets that accomplish the mapping $\mathbf{X} \rightarrow \mathbf{Y}$. A Bayesian prediction for some unseen test input \mathbf{x}^* correspondingly results from marginalizing the likelihood over the posterior distribution of the parameters

$$p(\mathbf{y}^* | \mathbf{x}^*, \mathbf{Y}, \mathbf{X}) = \int d\boldsymbol{\theta} p(\mathbf{y}^* | \mathbf{x}^*, \boldsymbol{\theta}) p(\boldsymbol{\theta} | \mathbf{Y}, \mathbf{X}). \quad (2)$$

Inserting Eq. (1) into Eq. (2) yields the predictive distribution

$$p(\mathbf{y}^* | \mathbf{x}^*, \mathbf{Y}, \mathbf{X}) = \frac{p(\mathbf{y}^*, \mathbf{Y} | \mathbf{x}^*, \mathbf{X})}{p(\mathbf{Y} | \mathbf{X})} \quad (3)$$

that depends on the model-dependent *network priors*

$$p(\mathbf{Y} | \mathbf{X}) = \int d\boldsymbol{\theta} p(\mathbf{Y} | \mathbf{X}, \boldsymbol{\theta}) p(\boldsymbol{\theta}), \quad (4)$$

$$p(\mathbf{y}^*, \mathbf{Y} | \mathbf{x}^*, \mathbf{X}) = \int d\boldsymbol{\theta} p(\mathbf{y}^* | \mathbf{x}^*, \boldsymbol{\theta}) p(\mathbf{Y} | \mathbf{X}, \boldsymbol{\theta}) p(\boldsymbol{\theta}). \quad (5)$$

The network priors encompass all input-output relationships which are compatible with the prior $p(\boldsymbol{\theta})$ and the model. The difference between the two network priors, Eq. (4) and Eq. (5), is the information on the additional test input \mathbf{x}^* and output \mathbf{y}^* .

Note that the Bayesian approach to supervised learning can also be used for input sequences $\{\mathbf{x}^{(0)}, \dots, \mathbf{x}^{(A)}\}$ with $\mathbf{x}^{(a)} \in \mathbb{R}^{n_{\text{in}}}$. To this end, it is sufficient to replace $\mathbf{x} \rightarrow \{\mathbf{x}^{(0)}, \dots, \mathbf{x}^{(A)}\}$ and $\mathbf{X} \rightarrow \{\mathbf{X}^{(0)}, \dots, \mathbf{X}^{(A)}\}$ in the above formulas.

The main difference between Bayesian inference and conventional, gradient-based training is that in the former one considers an entire ensemble of networks defined by the posterior distribution of the parameters while in the latter one seeks a point estimate $\hat{\boldsymbol{\theta}}$ for the parameters. Moreover, in the latter approach, learning refers to the process of refining initial single parameter estimates $\hat{\boldsymbol{\theta}}_0 \rightarrow \hat{\boldsymbol{\theta}}$ for the approximate posterior $p(\boldsymbol{\theta} | \mathbf{Y}, \mathbf{X}) \approx \delta(\boldsymbol{\theta} - \hat{\boldsymbol{\theta}}(\mathbf{Y}, \mathbf{X}, \mathcal{L}))$ by minimizing a loss \mathcal{L} on the set of training data \mathbf{Y}, \mathbf{X} . From the point of view of Bayesian inference, for a posterior that is sharply peaked at parameter value $\hat{\boldsymbol{\theta}}$, a Laplace approximation leads to a prediction based on the maximum a posteriori estimate, $p(\mathbf{y}^* | \mathbf{x}^*, \mathbf{Y}, \mathbf{X}) \approx p(\mathbf{y}^* | \mathbf{x}^*, \hat{\boldsymbol{\theta}})$. Thus, if $\hat{\boldsymbol{\theta}}$ corresponds to the parameter value found by conventional training, the Bayesian prediction and the prediction based on conventional training coincide.

In the following, we use a field theoretic approach to calculate the network priors for both deep and recurrent neural networks. Conditioning on the training data, Eq. (3), then yields the Bayesian prediction of the output.

2.2. Network architectures

Deep feedforward neural networks (DNNs) and discrete-time recurrent neural networks (RNNs) can both be described by a set of pre-activations $\mathbf{h}^{(a)} \in \mathbb{R}^{n_a}$ that are determined by an affine linear transformation

$$\mathbf{h}^{(a)} = \mathbf{W}^{(a)} \phi(\mathbf{h}^{(a-1)}) + \mathbf{W}^{(\text{in},a)} \mathbf{x}^{(a)} + \boldsymbol{\xi}^{(a)} \quad (6)$$

of activations $\phi(\mathbf{h}^{(a-1)}) \in \mathbb{R}^{n_a}$. The pre-activations are transformed by an activation function $\phi : \mathbb{R} \rightarrow \mathbb{R}$ which is applied element-wise to vectors. For DNNs, $\mathbf{W}^{(a)} \in \mathbb{R}^{n_a \times n_{a-1}}$ denotes the weight matrix from layer $a - 1$ to layer a , and $\boldsymbol{\xi}^{(a)} \in \mathbb{R}^{n_a}$ represents biases in layer a . Inputs $\mathbf{x}^{(a)}$ are typically only applied to the first layer such that the input matrices $\mathbf{W}^{(\text{in},a)} \in \mathbb{R}^{n_a \times n_{\text{in}}}$ vanish for $a > 0$. For RNNs, the index a denotes different time steps. The weight matrix, input matrix, and biases are static over time, $\mathbf{W}^{(a)} \equiv \mathbf{W}$, $\mathbf{W}^{(\text{in},a)} \equiv \mathbf{W}^{(\text{in})}$, and $\boldsymbol{\xi}^{(a)} \equiv \boldsymbol{\xi}$, and couple activities across successive time steps. For both architectures, we include an additional input and output layer

$$\mathbf{h}^{(0)} = \mathbf{W}^{(\text{in},0)} \mathbf{x}^{(0)} + \boldsymbol{\xi}^{(0)}, \quad (7)$$

$$\mathbf{y} = \mathbf{W}^{(\text{out})} \phi(\mathbf{h}^{(A)}) + \boldsymbol{\xi}^{(A+1)}, \quad (8)$$

with $\mathbf{W}^{(\text{out})} \in \mathbb{R}^{n_{\text{out}} \times n_A}$, which allow us to set independent input and output dimensions. Here, A denotes the final layer for the DNN and the final time point for the RNN. The set of parameters $\boldsymbol{\theta}$ is the collection of $\mathbf{W}^{(\text{in},a)}$, $\mathbf{W}^{(\text{out})}$, $\mathbf{W}^{(a)}$, and $\boldsymbol{\xi}^{(a)}$.

2.3. Parameter priors

We use Gaussian priors for all model parameters, that is for the RNN

$$W_{ij} \stackrel{\text{i.i.d.}}{\sim} \mathcal{N}(0, n^{-1}g^2), \quad (9)$$

$$W_{ij}^{(\text{in})} \stackrel{\text{i.i.d.}}{\sim} \mathcal{N}(0, n_{\text{in}}^{-1}g_0^2), \quad (10)$$

$$\xi_i \stackrel{\text{i.i.d.}}{\sim} \mathcal{N}(0, \sigma^2), \quad (11)$$

and for the DNN

$$W_{ij}^{(a)} \stackrel{\text{i.i.d.}}{\sim} \mathcal{N}(0, n_{a-1}^{-1}g_a^2), \quad (12)$$

$$W_{ij}^{(\text{in},a)} \stackrel{\text{i.i.d.}}{\sim} \mathcal{N}(0, n_{\text{in}}^{-1}g_0^2), \quad (13)$$

$$\xi_i^{(a)} \stackrel{\text{i.i.d.}}{\sim} \mathcal{N}(0, \sigma_a^2), \quad (14)$$

as well as

$$W_{ij}^{(\text{out})} \stackrel{\text{i.i.d.}}{\sim} \mathcal{N}(0, n_A^{-1}g_{A+1}^2), \quad (15)$$

$$\xi_i^{(A+1)} \stackrel{\text{i.i.d.}}{\sim} \mathcal{N}(0, \sigma_{A+1}^2), \quad (16)$$

for both architectures (where $n_A = n$ for the RNN). These priors on the parameters are used to calculate the network prior $p(\mathbf{Y} | \mathbf{X})$.

3. Unified field theoretical approach to RNNs and DNNs

The network prior $p(\mathbf{Y} | \mathbf{X})$, Eq. (4), is a joint distribution of all outputs $\mathbf{y}_\alpha \in \mathbf{Y}$, each corresponding to a single training input $\mathbf{x}_\alpha \in \mathbf{X}$. Its calculation is tantamount to a known problem in physics, the replica calculation [43, 46]. Here, each replicon is a copy of the network with the same parameters $\boldsymbol{\theta}$ but a different input \mathbf{x}_α . For simplicity, in the following we illustrate the derivation of $p(\mathbf{y} | \mathbf{x})$ for a single input $\mathbf{x} \equiv \mathbf{x}^{(a=0)}$ that is presented to the first layer of the DNN or at the first time point for the RNN, respectively. We present the more cumbersome but conceptually similar general case of multiple inputs, or multiple input sequences, in Appendix 6.1.

The network prior is defined as the probability of the output given the input,

$$p(\mathbf{y} | \mathbf{x}) = \int d\boldsymbol{\theta} p(\mathbf{y} | \mathbf{x}, \boldsymbol{\theta}) p(\boldsymbol{\theta}), \quad (17)$$

marginalized over the parameter prior, where

$$\begin{aligned} p(\mathbf{y} | \mathbf{x}, \boldsymbol{\theta}) &= \int d\mathbf{h}^{(0)} \dots \int d\mathbf{h}^{(A)} \delta\left(\mathbf{y} - \mathbf{W}^{(\text{out})}\boldsymbol{\phi}^{(A)} - \boldsymbol{\xi}^{(A+1)}\right) \\ &\quad \times \prod_{a=1}^A \delta\left(\mathbf{h}^{(a)} - \mathbf{W}^{(a)}\boldsymbol{\phi}^{(a-1)} - \boldsymbol{\xi}^{(a)}\right) \\ &\quad \times \delta\left(\mathbf{h}^{(0)} - \mathbf{W}^{(\text{in})}\mathbf{x} - \boldsymbol{\xi}^{(0)}\right), \end{aligned} \quad (18)$$

follows by enforcing the set of equations, Eq. (6) to Eq. (8), using Dirac constraints. Throughout the manuscript, we use the abbreviation $\boldsymbol{\phi}^{(a)} = \boldsymbol{\phi}(\mathbf{h}^{(a)})$.

3.1. Marginalization of the parameter prior

From Eq. (18), it follows that the computation of the marginalization of the parameters $\boldsymbol{\theta}$ in Eq. (17) can be reduced to

$$\begin{aligned} p(\mathbf{y} | \mathbf{x}) &= \int d\mathbf{h}^{(0)} \dots \int d\mathbf{h}^{(A)} \\ &\times \left\langle \delta \left(\mathbf{y} - \mathbf{W}^{(\text{out})} \boldsymbol{\phi}^{(A)} - \boldsymbol{\xi}^{(A+1)} \right) \right\rangle_{\mathbf{W}^{(\text{out})}, \boldsymbol{\xi}^{(A+1)}} \\ &\times \left\langle \left\langle \prod_{a=1}^A \delta \left(\mathbf{h}^{(a)} - \mathbf{W}^{(a)} \boldsymbol{\phi}^{(a-1)} - \boldsymbol{\xi}^{(a)} \right) \right\rangle_{\{\mathbf{W}^{(a)}\}} \right\rangle \\ &\times \left\langle \delta \left(\mathbf{h}^{(0)} - \mathbf{W}^{(\text{in})} \mathbf{x} - \boldsymbol{\xi}^{(0)} \right) \right\rangle_{\mathbf{W}^{(\text{in})}} \Big|_{\{\boldsymbol{\xi}^{(a)}\}}. \end{aligned} \quad (19)$$

To proceed, it is advantageous to represent the Dirac δ -distributions as Fourier integrals,

$$\delta(\mathbf{h}) = \int d\tilde{\mathbf{h}} \exp(\tilde{\mathbf{h}}^T \mathbf{h}) \quad (20)$$

with the inner product $\tilde{\mathbf{h}}^T \mathbf{h} = \sum_k \tilde{h}_k h_k$ and $\int d\tilde{\mathbf{h}} = \prod_k \int_{i\mathbb{R}} \frac{d\tilde{h}_k}{2\pi i}$, because it leads to averages of the form $\langle \exp(k\theta) \rangle_\theta$ which are analytically solvable. Using $\langle \exp(k\theta) \rangle_\theta = \exp(\frac{1}{2}\sigma^2 k^2)$ for $\theta \sim \mathcal{N}(0, \sigma^2)$, the network prior for a single replicon, $p(\mathbf{y} | \mathbf{x})$, takes the form (details in Appendix 6.1)

$$p(\mathbf{y} | \mathbf{x}) = \int d\tilde{\mathbf{y}} \int \mathcal{D}\mathbf{h} \int \mathcal{D}\tilde{\mathbf{h}} \exp(\mathcal{S}(\mathbf{y}, \tilde{\mathbf{y}}, \mathbf{h}, \tilde{\mathbf{h}} | \mathbf{x})), \quad (21)$$

where $\int \mathcal{D}\mathbf{h} \equiv \prod_{a=0}^A \prod_k \int_{\mathbb{R}} dh_k^{(a)}$ and $\int \mathcal{D}\tilde{\mathbf{h}} \equiv \prod_{a=0}^A \prod_k \int_{i\mathbb{R}} \frac{d\tilde{h}_k^{(a)}}{2\pi i}$. The exponent \mathcal{S} , commonly called *the action*, is given by

$$\mathcal{S}(\mathbf{y}, \tilde{\mathbf{y}}, \mathbf{h}, \tilde{\mathbf{h}} | \mathbf{x}) = \mathcal{S}_{\text{out}}(\mathbf{y}, \tilde{\mathbf{y}} | \mathbf{h}^{(A)}) + \mathcal{S}_{\text{net}}(\mathbf{h}, \tilde{\mathbf{h}} | \mathbf{x}), \quad (22)$$

where

$$\begin{aligned} \mathcal{S}_{\text{net}}(\mathbf{h}, \tilde{\mathbf{h}} | \mathbf{x}) &:= \sum_{a=0}^A \tilde{\mathbf{h}}^{(a)T} \mathbf{h}^{(a)} + \frac{1}{2} \sum_{a,b=0}^A \sigma_a^2 \tilde{\mathbf{h}}^{(a)T} M_{a,b} \tilde{\mathbf{h}}^{(b)} \\ &+ \frac{1}{2} \sum_{a,b=1}^A \frac{g_a^2}{n_{a-1}} \tilde{\mathbf{h}}^{(a)T} \boldsymbol{\phi}^{(a-1)T} M_{a,b} \boldsymbol{\phi}^{(b-1)} \tilde{\mathbf{h}}^{(b)} \\ &+ \frac{g_0^2}{2n_{\text{in}}} \tilde{\mathbf{h}}^{(0)T} \mathbf{x}^T \mathbf{x} \tilde{\mathbf{h}}^{(0)} \end{aligned} \quad (23)$$

is the action of the input and the recurrent layer of the RNN or the inner part of the DNN, respectively, and

$$\mathcal{S}_{\text{out}}(\mathbf{y}, \tilde{\mathbf{y}} | \mathbf{h}^{(A)}) := \tilde{\mathbf{y}}^T \mathbf{y} + \frac{\sigma_{A+1}^2}{2} \tilde{\mathbf{y}}^T \tilde{\mathbf{y}} + \frac{g_{A+1}^2}{2n_A} \tilde{\mathbf{y}}^T \boldsymbol{\phi}^{(A)T} \boldsymbol{\phi}^{(A)} \tilde{\mathbf{y}} \quad (24)$$

is the action for the output layer. Note that \mathcal{S} is diagonal in neuron indices with respect to the explicitly appearing fields \mathbf{h} and $\tilde{\mathbf{h}}$ and couplings across neurons are only mediated by terms of the form $\propto \boldsymbol{\phi}^T \boldsymbol{\phi}$.

For RNNs, the shared connectivity and biases at different time points imply correlations across time steps; for DNNs, in contrast, the connectivity and biases are

realized independently across layers, so that the action decomposes into a sum of $A+2$ individual layers. In Eq. (23), this leads to

$$M_{a,b} = \begin{cases} 1 & \text{RNN} \\ \delta_{a,b} & \text{DNN} \end{cases} \quad (25)$$

which is the only difference between DNN and RNN in this formalism.

3.2. Auxiliary variables

An action that is quadratic in \mathbf{h} and $\tilde{\mathbf{h}}$ corresponds to a Gaussian and therefore to an analytically solvable integral. However, the post-activations $\phi \equiv \phi(\mathbf{h})$ in \mathcal{S}_{net} and \mathcal{S}_{out} introduce a non-quadratic part and the terms $\propto \tilde{\mathbf{h}}^T \tilde{\mathbf{h}} \phi^T \phi$ cause a coupling across neurons. To deal with this difficulty, we introduce new auxiliary variables

$$C^{(a,b)} := M_{a,b} \left[\sigma_a^2 + \mathbb{1}_{a \geq 1, b \geq 1} \frac{g_a^2}{n_{a-1}} \phi^{(a-1)T} \phi^{(b-1)} \right] + \mathbb{1}_{a=0, b=0} \frac{g_0^2}{n_{\text{in}}} \mathbf{x}^T \mathbf{x}, \quad (26)$$

where $0 \leq a, b \leq A+1$, a common practice originating from dynamic spin-glass theory [47] and used for random networks [34–36, 48]. The second term $\propto \phi^T \phi$ in Eq. (26) contains the sum of post-activations over all neuron indices, where the indicator function $\mathbb{1}$ is 1 if both conditions in the subscripts are fulfilled and 0 otherwise. Assuming sufficiently weak correlations among the ϕ_i , we expect the sum to be close to its mean value with decreasing variations as n_a grows; for large n_a the sum is thus close to a Gaussian. This intuition is made precise below by a formal saddle point approximation in C .

Enforcing the auxiliary variables through Dirac- δ constraints, analogous to Eq. (20) (see Appendix 6.1 for details), leads to the prior distribution

$$p(\mathbf{y} | \mathbf{x}) = \int d\tilde{\mathbf{y}} \exp(\tilde{\mathbf{y}}^T \mathbf{y}) \left\langle \exp\left(\frac{1}{2} \tilde{\mathbf{y}}^T C^{(A+1, A+1)} \tilde{\mathbf{y}}\right) \right\rangle_{C, \tilde{C}}, \quad (27)$$

where the distribution $C, \tilde{C} \sim \exp(\mathcal{S}_{\text{aux}}(C, \tilde{C}))$ is described by the action

$$\mathcal{S}_{\text{aux}}(C, \tilde{C}) := -n \sum_{a,b=0}^{A+1} \nu_{a-1} \tilde{C}^{(a,b)} C^{(a,b)} + n \mathcal{W}_{\text{aux}}(\tilde{C} | C). \quad (28)$$

To account for possible differences in layer widths in DNNs, we here introduce $\nu_a = n_a/n = \mathcal{O}(1)$ as the relative network widths with respect to some reference n . For RNNs, all layers have the same width so that $\nu_{a>0} = 1$. For the input we have $\nu_{-1} \equiv n_{\text{in}}$. Lastly, we assume that the output size n_{out} does not scale with n , i.e., $n_{\text{out}} = \mathcal{O}(1)$, such that the only $\mathcal{O}(n)$ contribution in the $\langle \cdot \rangle_{C, \tilde{C}}$ expectation in Eq. (27) is due to Eq. (28). The recurrent part and the input, which decouple in the neurons, are together described for the DNN by

$$\begin{aligned} \mathcal{W}_{\text{aux}}^{\text{DNN}}(\tilde{C} | C) &= \sum_{a=1}^{A+1} \nu_{a-1} \ln \left\langle e^{\tilde{C}^{(a,a)} g_a^2 \phi^{(a-1)} \phi^{(a-1)}} \right\rangle_{h^{(a-1)}} \\ &\quad + \nu_{-1} \tilde{C}^{(0,0)} \frac{g_0^2}{n_{\text{in}}} \mathbf{x}^T \mathbf{x} + \sum_{a=0}^{A+1} \nu_{a-1} \tilde{C}^{(a,a)} \sigma_a^2 \end{aligned} \quad (29)$$

with $h^{(a)} \sim \mathcal{N}(0, C^{(a,a)})$ a scalar centered Gaussian with layer-dependent variance $\langle h^{(a)} h^{(a)} \rangle = C^{(a,a)}$ and for the RNN by

$$\begin{aligned} \mathcal{W}_{\text{aux}}^{\text{RNN}}(\tilde{C} | C) &= \ln \left\langle e^{\sum_{a,b=1}^{A+1} \tilde{C}^{(a,b)} g^2 \phi^{(a-1)} \phi^{(b-1)}} \right\rangle_{\{h^{(a)}\}} \\ &\quad + \nu_{-1} \tilde{C}^{(0,0)} \frac{g_0^2}{n_{\text{in}}} \mathbf{x}^T \mathbf{x} + \sum_{a,b=0}^{A+1} \tilde{C}^{(a,b)} \sigma^2 \end{aligned} \quad (30)$$

with $\{h^{(a)}\} \equiv \{h^{(a)}\}_{0 \leq a \leq A}$ and $\{h^{(a)}\}_{0 \leq a \leq A} \sim \mathcal{N}(0, C)$ a scalar centered Gaussian across time with covariance matrix $\langle h^{(a)} h^{(b)} \rangle = C^{(a,b)}$. Note that the ϕ in (29) and (30) are one-dimensional with regard to the neuron index, since the system is homogeneous across neurons after the disorder average; the number of neurons is contained in the prefactor n in (28) and in the factors ν_a in (29).

3.3. Saddle-point approximation

The factor n in Eq. (28), which stems from the decoupling across neurons, for large n leads to a strongly peaked distribution of C and \tilde{C} . Therefore we can use a saddle point approximation to calculate the average over C and \tilde{C} in Eq. (27). In the limit $n \rightarrow \infty$ this approximation becomes exact.

We thus search for stationary points of the action

$$\begin{aligned} \frac{\partial}{\partial C^{(a,b)}} \mathcal{S}_{\text{aux}}(C, \tilde{C}) &\stackrel{!}{=} 0, \\ \frac{\partial}{\partial \tilde{C}^{(a,b)}} \mathcal{S}_{\text{aux}}(C, \tilde{C}) &\stackrel{!}{=} 0, \end{aligned} \quad (31)$$

which yields a coupled set of self-consistency equations for the mean values \bar{C} and $\bar{\tilde{C}}$, commonly called mean-field equations: $\bar{\tilde{C}}^{(a,b)} \equiv 0$, which follows from the normalization of the probability distribution [49], and

$$\begin{aligned} \bar{C}^{(a,b)} &= M_{a,b} \left[\sigma_a^2 + \mathbb{1}_{a \geq 1, b \geq 1} g_a^2 \langle \phi(h^{(a-1)}) \phi(h^{(b-1)}) \rangle_{h^{(a-1)}, h^{(b-1)}} \right] \\ &\quad + \mathbb{1}_{a=0, b=0} \frac{g_0^2}{n_{\text{in}}} \mathbf{x}^T \mathbf{x} \end{aligned} \quad (32)$$

with $h^{(a-1)}, h^{(b-1)} \sim \mathcal{N}(0, \bar{C})$. Eq. (32) comprises both DNN and RNN; the difference between Eq. (29) and Eq. (30) leads to the appearance of $M_{a,b}$ on the r.h.s. The average on the r.h.s. has to be taken with respect to a probability distribution that only includes two layers or time points. This is due to the marginalization property of the Gaussian distribution of the pre-activations $h^{(a-1)}$, which results from inserting the saddle-point solutions Eq. (32) for \bar{C} and $\bar{\tilde{C}}$. Accordingly, we are left with a closed system of equations for the saddle-point values \bar{C} that are the layer- or time-dependent correlations. These equations need to be solved recursively from the input $\bar{C}^{(0,0)} = \sigma_0^2 + \frac{g_0^2}{n_{\text{in}}} \mathbf{x}^T \mathbf{x}$ to the output $\bar{C}^{(A+1, A+1)} = \sigma_{A+1}^2 + g_{A+1}^2 \langle \phi(h^{(A)}) \phi(h^{(A)}) \rangle_{h^{(A)}, h^{(A)}}$.

3.4. Network prior

Computing the Gaussian integral over $\tilde{\mathbf{y}}$ in the saddle-point approximation of Eq. (27), one obtains the distribution of the outputs as independent Gaussians across neurons i

$$p(\mathbf{y} | \mathbf{x}) = \prod_i p(y_i | \mathbf{x}) = \prod_i \mathcal{N}(y_i; 0, \overline{C}^{(A+1, A+1)}). \quad (33)$$

An analogous calculation for multiple input sequences $\{\mathbf{x}_\alpha^{(0)}, \dots, \mathbf{x}_\alpha^{(A)}\}$ (see Appendix 6.1) yields the equivalent mean-field equations

$$\begin{aligned} \overline{C}_{\alpha\beta}^{(a,b)} = M_{a,b} & \left[\sigma_a^2 + \mathbb{1}_{a \geq 1, b \geq 1} g_a^2 \langle \phi(h_\alpha^{(a-1)}) \phi(h_\beta^{(b-1)}) \rangle_{h_\alpha^{(a-1)}, h_\beta^{(b-1)}} \right. \\ & \left. + \mathbb{1}_{a \leq A, b \leq A} \frac{g_0^2}{n_{\text{in}}} \mathbf{x}_\alpha^{(a)\text{T}} \mathbf{x}_\beta^{(b)} \right] \end{aligned} \quad (34)$$

with $h_\alpha^{(a-1)}, h_\beta^{(b-1)} \sim \mathcal{N}(0, \overline{C})$ and $0 \leq a, b \leq A + 1$. These lead to the joint network prior

$$\begin{aligned} p(\mathbf{Y} | \{\mathbf{X}^{(0)}, \dots, \mathbf{X}^{(A)}\}) &= \prod_i p(\mathbf{y}_i | \{\mathbf{X}^{(0)}, \dots, \mathbf{X}^{(A)}\}) \\ &= \prod_i \mathcal{N}(\mathbf{y}_i; 0, \mathbf{K}) \end{aligned} \quad (35)$$

where the covariance matrix is the Gram matrix of the kernel [30],

$$\mathbf{K}_{\alpha\beta} = \overline{C}_{\alpha,\beta}^{(A+1, A+1)}. \quad (36)$$

Here \mathbf{y}_i denotes the i -th row of the output matrix \mathbf{Y} that comprises the output of neuron i to all input sequences $\{\mathbf{x}_\alpha^{(0)}, \dots, \mathbf{x}_\alpha^{(A)}\}$.

In principle, it is also possible to use independent biases or input weights across time steps in the RNN. This would lead to the respective replacements $M_{a,b}\sigma^2 \rightarrow \delta_{a,b}\sigma^2$ and $M_{a,b}\mathbb{1}_{a \leq A, b \leq A} \frac{g_0^2}{n_{\text{in}}} \mathbf{x}_\alpha^{(a)\text{T}} \mathbf{x}_\beta^{(b)} \rightarrow \delta_{a,b}\mathbb{1}_{a \leq A, b \leq A} \frac{g_0^2}{n_{\text{in}}} \mathbf{x}_\alpha^{(a)\text{T}} \mathbf{x}_\beta^{(b)}$ in Eq. (34).

3.5. Predictive distribution

We split \mathbf{X}, \mathbf{Y} into training data (indexed by subscript D) and test data (indexed by subscript $*$). The conditioning on the training data via Eq. (3) can here be done analytically because the network priors are Gaussian [30]. For scalar inputs, this yields the predictive distribution

$$p(\mathbf{Y}_* | \mathbf{X}_*, \mathbf{Y}_D, \mathbf{X}_D) = \prod_i \mathcal{N}(\mathbf{y}_{*i}; \boldsymbol{\mu}_{GP}, \mathbf{K}_{GP}) \quad (37)$$

with

$$\boldsymbol{\mu}_{GP} = \mathbf{K}_{*D} \mathbf{K}_{DD}^{-1} \mathbf{y}_D, \quad \mathbf{K}_{GP} = \mathbf{K}_{**} - \mathbf{K}_{*D} \mathbf{K}_{DD}^{-1} \mathbf{K}_{*D}^T, \quad (38)$$

which are fully determined by the kernel matrix $\mathbf{K} = \begin{pmatrix} \mathbf{K}_{DD} & \mathbf{K}_{*D}^T \\ \mathbf{K}_{*D} & \mathbf{K}_{DD} \end{pmatrix}$. For input sequences, it is again sufficient to replace $\mathbf{X}_* \rightarrow \{\mathbf{X}_*^{(0)}, \dots, \mathbf{X}_*^{(A)}\}$ and $\mathbf{X}_D \rightarrow \{\mathbf{X}_D^{(0)}, \dots, \mathbf{X}_D^{(A)}\}$.

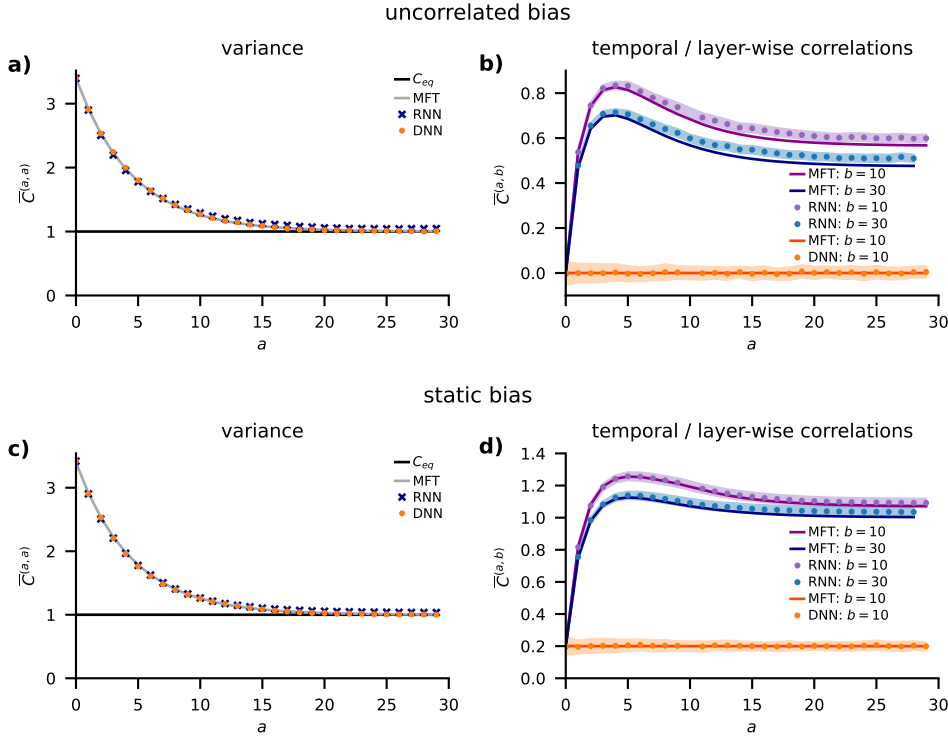


Figure 1. Mean-field theory for DNN and RNN with a single input. **a)** Average variance in mean-field theory $\overline{C}^{(a,a)}$ (Eq. (32); solid gray curve) and estimate $\frac{1}{n_a} \sum_i h_i^{(a)} h_i^{(a)}$ from simulation, averaged over 100 realizations of networks, for biases that are uncorrelated across time/layers (blue crosses RNN; orange dots DNN). **b)** Cross-covariance $\overline{C}^{(a,b)}$ as a function of the hidden layer index a for fixed $b \in \{10, 30\}$ and uncorrelated biases. RNN: Mean-field theory (solid dark blue and dark magenta). Mean (blue / purple dots) and standard error of the mean (light blue / light purple tube) of $\frac{1}{n_a} \sum_i h_i^{(a)} h_i^{(b)}$ estimated from simulation of 100 network realizations. DNN: Mean (orange dots) and standard error of the mean of $\frac{1}{n_a} \sum_i h_i^{(a)} h_i^{(b)}$ estimated from simulation of 100 network realizations. Other parameters $g_0^2 = g^2 = 1.6$, $\sigma^2 = 0.2$, finite layer width $n_a = 2000$, $A = 30$ hidden layers, ReLU activation $\phi(x) = \max(0, x)$ and Gaussian inputs $\mathbf{x} \stackrel{\text{i.i.d.}}{\sim} \mathcal{N}(1, 1)$ with $n_{\text{in}} = 10^5$. **c)** Same as a) but for biases that are static across time/layers. **d)** Same as b) but for the static bias case.

4. Comparison of RNNs and DNNs

Above, we derived the mean-field equations (34) for the kernel matrix \mathbf{K} using a field-theoretic approach. Here, we investigate differences in the mean-field distributions of the different network architectures, starting with the kernel and considering the predictive distribution afterwards.

4.1. Kernel

The diagonal elements, $\overline{C}^{(a,a)}$ for the single-input case in Eq. (32) and equivalently $\overline{C}_{\alpha,\beta}^{(a,a)}$ for the multiple-input-sequences case in Eq. (34), are identical for RNNs and DNNs, because $M_{a,a} = 1$ for both architectures. This implies that the equal-time or within-layer statistics, correspondingly, is the same in both architectures. The reason is that the iterations Eq. (32) and Eq. (34) for equal-time points $a = b$ form closed sets of equations; they can be solved independently of the statistics for different time points $a \neq b$. Formally, this follows from the marginalization property of the Gaussian, which implies that any subset of a multivariate Gaussian is Gaussian, too, with a covariance matrix that is the corresponding sector of the covariance matrix of all variables [30]. The precise agreement of this mean-field prediction with the average correlation estimated from direct simulation is shown in Figure 1a and c for the single-input case for both uncorrelated (a) and static biases (c) across time or layers, respectively.

A notable difference between RNN and DNN is that activity in the RNN is correlated across time steps due to the shared weights, even if biases are uncorrelated in time, as shown in Figure 1b. Static biases simply strengthen the correlations across time steps (see Figure 1d). For DNNs, in contrast, cross-layer correlations only arise due to biases that are correlated across layers, because weights are drawn independently for each layer. This is shown in Figure 1b and d: Correlations vanish for DNNs in the uncorrelated bias case (b) and take on the value σ^2 , the variance of the bias, in the static bias case (d). Again, the mean-field theory accurately predicts the non-zero correlations across time in the RNN as well as the correlations across layers generated by the correlated biases in the DNN. In the RNN, temporal correlations show a non-trivial interplay due to the shared weights across time. We observe an instability that can build up by this mechanism in finite-size RNNs, even in parameter regimes that are deemed stable in mean-field theory (see Appendix 6.2, Figure 4).

In a particular case, the correlations across time steps also vanish for the RNN: we show by induction that off-diagonal elements vanish for point-symmetric activation functions if inputs are only provided in the initial time step, $\{\mathbf{X}^{(0)}, 0, \dots, 0\} \equiv \mathbf{X}$, and the bias is absent, $\sigma = 0$ (or uncorrelated across time steps). Assuming that $\overline{C}_{\alpha,\beta}^{(a-1,b-1)} \stackrel{a \neq b}{=} 0$, we have

$$\overline{C}_{\alpha,\beta}^{(a,b)} = g^2 \langle \phi(h_\alpha^{(a-1)}) \rangle_{h_\alpha^{(a-1)}} \langle \phi(h_\beta^{(b-1)}) \rangle_{h_\beta^{(b-1)}} \stackrel{\phi \text{ odd}}{=} 0 \quad (39)$$

with $h_\alpha^{(a-1)} \sim \mathcal{N}(0, \overline{C})$ and $h_\beta^{(b-1)} \sim \mathcal{N}(0, \overline{C})$. Hence, if the pre-activations $h_\alpha^{(a-1)}, h_\beta^{(b-1)}$ at points $a - 1$ and $b - 1$ are uncorrelated, also $h_\alpha^{(a)}, h_\beta^{(b)}$ will be uncorrelated. The base case of the induction proof follows from the independence of the input weights $\mathbf{W}^{(\text{in})}$ and the recurrent weights \mathbf{W} : Correlations between time point zero and other time points are zero. Therefore, by induction in time, time points will be uncorrelated at any point, meaning that for odd activations ϕ and the considered input layer, the solutions of the mean-field equations are the same for DNNs and RNNs. Figure 5 in the Appendix 6.3 is similar to Figure 1 but for the erf nonlinearity. There we observe the vanishing temporal correlation for RNNs with uncorrelated bias explicitly.

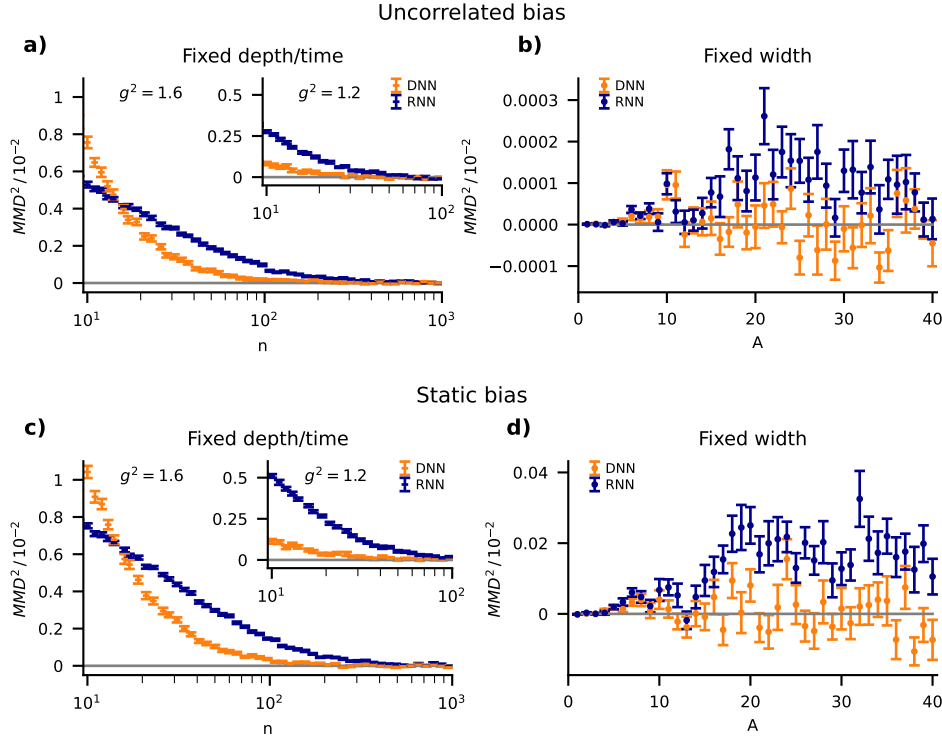


Figure 2. Convergence of RNN and DNN towards the mean-field theory. Maximum mean-discrepancy MMD^2 for a radial basis function kernel with length scale $l = 1/2$ [50] between the empirical distribution of scalar outputs y_α and the Gaussian distribution with covariance matrix $K_{\alpha\beta} = \overline{C}_{\alpha,\beta}^{(A+1,A+1)}$ predicted by MFT Eq. (34). Empirical MMD^2 estimation across 2000 realizations (W, ξ) . Average over 40 realizations of $\{\mathbf{x}_\alpha\}_{\alpha=1,\dots,10}$, $x_{\alpha,i} \stackrel{i.i.d.}{\sim} \mathcal{N}(0,1)$ and $\dim(\mathbf{x}_\alpha) = 4$ (error bars showing standard error of the mean). ReLU activation $\phi(x) = \max(0, x)$. **a)** MMD^2 as a function of the width of the network layer n for $g^2 = 1.6$ and $g^2 = 1.2$ (inset), with $A = 15$ and $\sigma^2 = 0.2$ and uncorrelated biases across time/layers. **b)** MMD^2 as a function of the depth or duration A , for width $n = 500$, $g^2 = 1.6$, and $\sigma^2 = 0.2$ and uncorrelated biases. **c)** Same as a) but for biases that are static across time/layers. **d)** Same as b) but for the static bias case.

4.2. Predictive distribution

Coming back to the general case, we next ask if the different off-diagonal elements of the mean-field equations for RNN and DNN have observable consequences. The answer is no if a linear readout is taken at a single time point or layer A , correspondingly (cf. Eq. (8) for the readout): This is a direct consequence of the identical diagonal elements of the covariance $\overline{C}_{\alpha,\beta}^{(a,a)}$, so that the predictive distribution Eq. (37) for the RNN and the DNN is identical in mean-field theory; the two architectures have the same Gram matrix $K_{\alpha\beta} = \overline{C}_{\alpha,\beta}^{(A+1,A+1)}$ and thus the same predictive distribution Eq. (37). This means that the two architectures have identical computational capabilities in the limit of infinite layer width.

To check how quickly the mean-field theory is approached by finite-size networks, we measure the maximum mean-discrepancy (MMD) [9, 50] between the Gaussian distribution with covariance matrix $K_{\alpha\beta}$ and the empirical joint distribution of a set of scalar outputs y_α , Eq. (8), across realizations of W and ξ . The inputs \mathbf{x}_α are random patterns presented to the first layer or time step, respectively. We find that convergence is rather fast for both architectures (Figure 2a and c). For sufficiently deep architectures $A \gg 1$ as well as both uncorrelated and static biases, RNNs systematically show a slower convergence than DNNs, which could be anticipated due to the smaller number of independently drawn Gaussian weights, N^2 versus AN^2 . This observation is in line with the MMD being larger for the RNN than for the DNN for $A \gtrsim 15$ (Figure 2b and d). This is also consistent with the coherent interplay of shared connectivity and correlated activity across time steps in the RNN (see Appendix 6.2, Figure 4). Overall, we find a faster convergence for uncorrelated biases than for biases that are static over time or layers, respectively.

The temporal correlations present in RNNs become relevant in the case of sequence processing. In such a setting, the network in each time step a receives a time dependent input $\mathbf{x}_\alpha^{(a)}$ with a non-trivial temporal correlation structure $\mathbf{x}_\alpha^{(a+\tau)\top} \mathbf{x}_\beta^{(a)}$ that drives the temporal correlations $\bar{C}_{\alpha,\beta}^{(a'+\tau,a')}$ of the RNN activations for $a' \geq a$, see Eq. (34). If the latter are read out in each time step, temporal correlations enter the kernel and thus influence task performance.

We finally note that we here use a separate readout layer. The realization of readout weights as independent Gaussian variables causes vanishing temporal correlations between the readouts and the activity in previous layers or time steps, respectively. For the Gaussian kernel, however, the presence or absence of a readout layer does not make any difference. Alternatively, the readout of n_{out} signals could be taken from an arbitrary choice of n_{out} neurons in the last layer or time step, respectively, leading to the same kernel.

4.3. Next-to-leading order corrections

The saddle point approximation finds the dominant value for the correlation $C^{(a,b)}$ by computing the stationary point of the action \mathcal{S}_{aux} given by Eq. (31). A standard way to go beyond the leading order is to obtain corrections of order $\mathcal{O}(n^{-1})$ by computing the Gaussian fluctuations of C and \tilde{C} around their saddle-point values. To this end, we need the Hessian matrix $\mathcal{S}_{\text{aux},ij}^{(a,b),(c,d)}$, i.e., the derivatives of \mathcal{S}_{aux} with respect to all combinations of $C^{(a,b)}$ and $\tilde{C}^{(c,d)}$. The computation is global in the sense that we consider the Hessian for all time points or layers, (a,b) , (c,d) , simultaneously. This is in contrast to existing perturbative approaches in DNNs, which proceed layer by layer [24, 25]. The negative inverse of the Hessian is the covariance matrix (or *propagator*) Δ ,

$$-\sum_{k=1}^2 \mathcal{S}_{\text{aux},ik} \Delta_{kj} = \delta_{i,j} \mathbf{1}, \quad (40)$$

which is meant as a 2x2 tensor equation consisting of tensors with four time indices (see Appendix 6.5 for details).

Due to the normalization $\mathcal{W}_{\text{aux}}(0|C) = 0$, given by (30) or (29), respectively, the Hessian has a zero in the upper left corner $\mathcal{S}_{\text{aux},11}^{(a,b),(c,d)} \equiv \partial^2 \mathcal{S}_{\text{aux}} / \partial C^{(a,b)} \partial C^{(c,d)} \equiv 0$. This implies a zero in the lower right corner of its inverse Δ . As a consequence,

the off-diagonal elements $\Delta_{12}^{(a,b),(c,d)} = \Delta_{21}^{(c,d),(a,b)}$, which are response functions and time-reversed (transposed) of one another, can be determined independently of Δ_{11} through

$$-\mathcal{S}_{\text{aux},12} \Delta_{21} = \mathbf{1}.$$

A direct calculation (Appendix 6.5) shows that for DNN and for RNN their equal-time entries $\Delta_{12}^{(a,a),(e,e)}$ are causal, i.e., they vanish for $a < e$, and are else given by

$$\Delta_{12}^{(a,a),(e,e)} = \langle C^{(a,a)} \tilde{C}^{(e,e)} \rangle = n^{-1} \nu_{e-1}^{-1} \prod_{k=e}^{a-1} F_k, \quad (41)$$

where $F_k = g_{k+1}^2 \partial \langle \phi^{(k)} \phi^{(k)} \rangle / \partial C^{(k,k)}$ is the linear response of the correlator $g_{k+1}^2 \langle \phi^{(k)} \phi^{(k)} \rangle$ in layer k with regard to changes of the variance $C^{(k,k)}$ of the latent variables in that layer; for RNN we have $\nu = 1$. With the ReLU non-linearity, F_k takes the particularly simple form $F_k = \frac{1}{2} g_{k+1}^2$. This implies that the response functions show exponentially decaying behavior for $g_k^2 < 2$, which is the stable regime of the mean-field equations.

The response function Δ_{12} describes how the variability δC of the variance in the first layer or time step 0 is propagated to a downstream layer or later time step a . Since the joint statistics of C and \tilde{C} follows $C, \tilde{C} \sim \exp(\mathcal{S}_{\text{aux}}(C, \tilde{C}))$, to linear order the variability δC in layer 0 affects the variability in layer a as

$$C^{(a,a)} = \langle C^{(a,a)} \rangle_{C^{(0,0)}=\tilde{C}^{(0,0)}} + \Delta_{12}^{(a,a),(0,0)} \delta C^{(0,0)} + \mathcal{O}(\delta^2), \quad (42)$$

where we used that $\partial \langle C^{(a,a)} \rangle_{C^{(0,0)}} / \partial C^{(0,0)} = \langle C^{(a,a)} \tilde{C}^{(0,0)} \rangle = \Delta_{12}^{(a,a),(0,0)}$. This can also be seen by noting that the solution (41) for Δ_{12} is identical to the linear response of the iterative mean-field equations (32) with regard to an infinitesimal perturbation of $C^{(e,e)}$.

The diagonal element $\Delta_{11}^{(a,a),(a,a)}$ of the propagator in (40) is the variability of the variance in layer a . Considering the other entries of (40), we find that it obeys (see also (64))

$$\Delta_{11} = \Delta_{12} \mathcal{S}_{\text{aux},22} \Delta_{21}, \quad (43)$$

where in

$$\begin{aligned} \mathcal{S}_{\text{aux},22}^{(a,b),(c,d)} &= \frac{\partial^2 \mathcal{S}_{\text{aux}}}{\partial \tilde{C}^{(a,b)} \partial \tilde{C}^{(c,d)}} \\ &= n \left\langle \phi^{(a-1)} \phi^{(b-1)}, \phi^{(c-1)} \phi^{(d-1)} \right\rangle_c \\ &\quad \times \begin{cases} g_a^4 \nu_{a-1} \delta_{a,b} \delta_{c,d} \delta_{a,c} & \text{DNN} \\ g^4 & \text{RNN} \end{cases} \\ &=: n G_{a-1,b-1,c-1,d-1}, \end{aligned}$$

the connected correlation function (second cumulant) $\langle \circ, \circ \rangle_c$ of $\phi\phi$ appears in the second line. The expression (43) shows that fluctuations generated by $\mathcal{S}_{\text{aux},22}^{(2)}$ propagate through the network forward in time or layer, expressed by the two factors Δ_{12} and Δ_{21} . The Kronecker δ in the expression for the DNN imply that fluctuations are intrinsically-generated only within layers, whereas in the RNN fluctuations between different time points are correlated due to the weight sharing. One is typically interested in the fluctuations measured in a single layer a , for example

in the readout layer. In this case due to $\Delta_{12}^{(a,a),(c,d)} \propto \delta_{c,d}$ and by (43), one only needs $\mathcal{S}_{\text{aux},22}^{(a,a),(c,c)}$ to obtain

$$\Delta_{11}^{(a,a),(a,a)} = n^{-1} \begin{cases} \sum_{a'=1}^a \left\{ \prod_{k=a'}^{a-1} F_k^2 \right\} \nu_{a'-1}^{-1} G_{a'-1,a'-1,a'-1,a'-1} \\ \sum_{a',c'=1}^a \left\{ \prod_{k=a'}^{a-1} F_k \right\} \left\{ \prod_{l=c'}^{a-1} F_l \right\} G_{a'-1,a'-1,c'-1,c'-1} \end{cases} \quad (44)$$

where the upper result holds for the DNN and the lower for the RNN. The two expressions differ by the presence of the additional summation index c' in the case of the RNN and by the appearance of the relative layer sizes ν for the DNN. The reason is, again, that correlated fluctuations in the RNN are generated also across different time steps due to weight sharing. A further difference is that F and G must be evaluated at the corresponding mean-field solutions of the two network architectures. For the ReLU activation function we find $G_{a-1,a-1,a-1,a-1} = \frac{5}{4}g_a^4 C^{(a-1,a-1)}C^{(a-1,a-1)}$ for the DNN as well as $G_{a-1,a-1,c-1,c-1} = g^4 \left(\langle \phi^{(a-1)} \phi^{(a-1)} \phi^{(c-1)} \phi^{(c-1)} \rangle - \frac{1}{4} C^{(a-1,a-1)} C^{(c-1,c-1)} \right)$ with $\langle \phi^{(a-1)} \phi^{(a-1)} \phi^{(c-1)} \phi^{(c-1)} \rangle$ known from [51] for the RNN (see Eq. (69)).

The comparison of the theoretical prediction (44) to an estimate of the fluctuations of C is shown in Figure 3. As expected for the next-to-leading order corrections being $\propto \mathcal{O}(n^{-1})$, the variability declines inversely proportional to n , as shown in Figure 3a. The variability for the RNN is throughout larger than for the DNN. This can be anticipated from the expression (44), which shows that for the RNN fluctuations of $\phi\phi$ across different time-steps $a' \neq c'$ drive fluctuations at the later final time point, while for the DNN only fluctuations from within the same layer a' are propagated forward to the final layer. As a function of depth (DNN) or time step (RNN), respectively, the fluctuation corrections show a characteristic form with an initial increase followed by a plateau, shown in Figure 3b. This is due to the exponential decay of the causal response functions $\Delta_{12}^{(a,a),(a',a')}$ with the distance $a - a'$ in (44). For a stationary mean-field solution one would have $F_k = F$, so the depth or time scale is $\tau = -(\ln F)^{-1}$, because $\Delta_{12}^{(a,a),(a',a')} \propto F^{a-a'} = e^{(a-a') \ln F} = e^{-\frac{a-a'}{\tau}}$. For ReLU activations this evaluates to $\tau = (\ln 2 - 2 \ln g)^{-1} \simeq 2$ for $g^2 = 1.2$. As expected, at the point $g^2 = 2$, where the mean-field solution loses stability, also this time scale diverges. The function Δ_{12}^2 appearing in (44) thus declines with about a unit scale for the given parameters. The initial increase of fluctuations Δ_{11} results from the convolution with Δ_{12}^2 of the variance of $\phi\phi$, which itself has a transient behavior inherited from the transient of the mean-field solution shown in Figure 1. At large depth, fluctuations saturate on a plateau, the height of which is given by the accumulated fluctuations of the previous layers, discounted by Δ_{12}^2 ; the driving fluctuations of $\phi\phi$ in this limit become constant as the mean-field solution \bar{C} approaches its stationary plateau. Since Δ_{12} has the same form for the RNN and the DNN, analog considerations explain the rise-and-plateau shape for the RNN.

Figure 3c and d show the propagation of fluctuations of the input through the layers of the DNN (c) and through time in the RNN (d). The simulations (dots) show good agreement with the theoretical prediction from linear response theory (42) (curves) for both architectures. In fact, the theoretical predictions for the statistics within a layer (DNN) and for equal times (RNN) are identical. One observes the exponential decay of the input variability with deeper layers or later time, respectively,

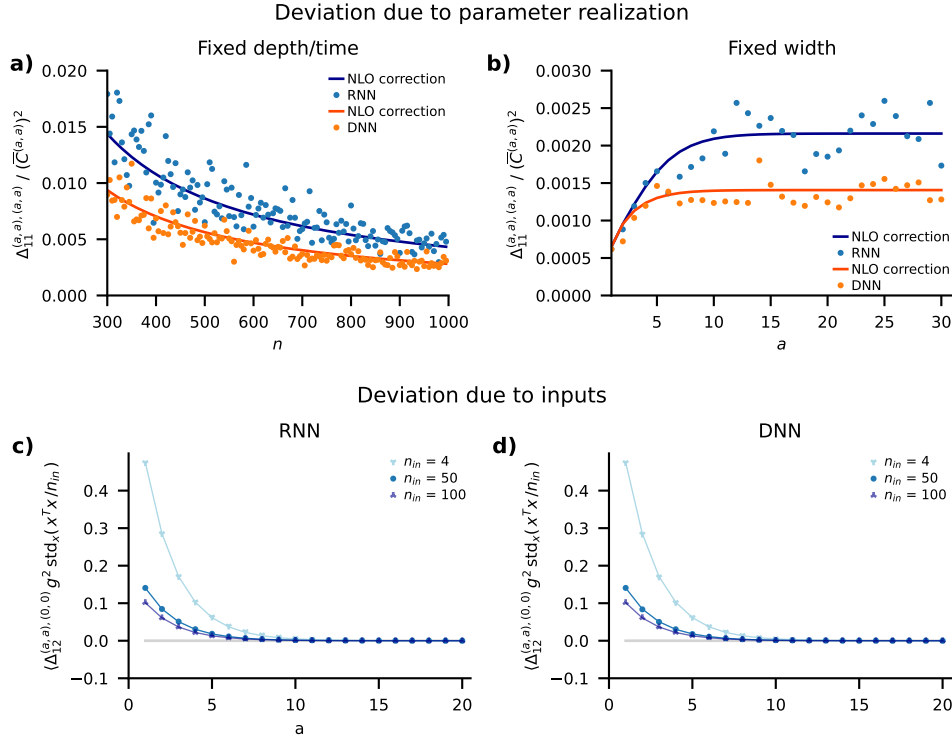


Figure 3. NLO corrections for DNN and RNN. Fluctuations $\Delta_{11}^{(a,a),(a,a)}$ of the covariance $C^{(a,a)}$ around its mean value $\bar{C}^{(a,a)}$ in the last layer $a = A + 1$ across realizations of weights W and biases ξ . **a)** $\Delta_{11}^{(a,a),(a,a)}$ for $a = A + 1$ as a function of the network width n ; simulations as dots, estimated across 100 realizations of W and ξ , and theoretical prediction (44) as curves for RNN (blue) and DNN (orange). Network parameters: $g^2 = g_a^2 = 1.2$, $\sigma^2 = \sigma_a^2 = 0.2$, $A = 15$. All realizations use the same fixed input $\mathbf{x} \in \mathbb{R}^4$ with $x_i \stackrel{\text{i.i.d.}}{\sim} \mathcal{N}(0,1)$ and ReLU activation $\phi(x) = \max(0, x)$. **b)** $\Delta_{11}^{(a,a),(a,a)}$ as a function of the network depth or readout time a , respectively; simulations as dots, estimated from 100 realizations of W and ξ , and theoretical prediction (44) as curves for RNN (blue) and DNN (orange). Network parameters: $g^2 = g_a^2 = 1.2$, $\sigma^2 = \sigma_a^2 = 0.2$ and $n = 2000$. Same input $\mathbf{x} \in \mathbb{R}^4$ with $x_i \stackrel{\text{i.i.d.}}{\sim} \mathcal{N}(0,1)$ and ReLU activation $\phi(x) = \max(0, x)$ as in panel a). **c)** RNN, **d)** DNN fluctuations of the mean field covariance induced by input fluctuations as a function of the layer / time step a . Dots represent the simulation result obtained as the standard deviation with respect to different input realizations x of the weight averaged overlaps $\bar{C}^{(a,a)}(\mathbf{x}) = \left\langle \frac{1}{n_a} \phi^{(a-1)\text{T}} \phi^{(a-1)} \right\rangle_W(\mathbf{x})$; we used 100 network realizations in the simulations. Lines represent the theoretical prediction based on linear response theory (42). Network parameters: $g^2 = g_a^2 = 1.2$, $\sigma^2 = \sigma_a^2 = 0.2$ and $n = 500$.

as pointed out above.

The fluctuations Δ_{11} yield a non-Gaussian distribution of the output of the network

$$\begin{aligned} p(\mathbf{y} | \mathbf{x}) &\simeq \int d\tilde{\mathbf{y}} \exp(\tilde{\mathbf{y}}^T \mathbf{y}) \left\langle \exp\left(\frac{1}{2} \tilde{\mathbf{y}}^T C \tilde{\mathbf{y}}\right) \right\rangle_{C \sim \mathcal{N}(\bar{C}, \Delta_{11})} \\ &= \int d\tilde{\mathbf{y}} \exp(\tilde{\mathbf{y}}^T \mathbf{y}) \exp\left(\frac{1}{2} \tilde{\mathbf{y}}^T \bar{C}^{(A+1, A+1)} \tilde{\mathbf{y}}\right) \\ &\quad + \frac{1}{8} \Delta_{11}^{(A+1, A+1), (A+1, A+1)} (\tilde{\mathbf{y}}^T \tilde{\mathbf{y}})^2. \end{aligned}$$

The latter term $\frac{1}{8} \Delta_{11}^{(A+1, A+1), (A+1, A+1)} (\tilde{\mathbf{y}}^T \tilde{\mathbf{y}})^2$ describes fourth order cumulants of the output y between pairs of indices i, j due to the appearance of $(\tilde{\mathbf{y}}^T \tilde{\mathbf{y}})^2 = \sum_{i, j} \tilde{y}_i^2 \tilde{y}_j^2$. This approximation may be combined with results by Zavatone-Veth et al. [24] or Naveh and Ringel [25] to obtain finite-size corrections for the statistics of the predictive distribution, extending their results to networks of arbitrary depth and to arbitrary activation functions.

5. Discussion

We present a unified derivation of the mean-field theory for deep (DNN) and recurrent neural networks (RNN) with arbitrary activation functions using field-theoretical methods. The derivation in particular yields the Gaussian process kernel that predicts the performance of networks trained in a Bayesian way. For the network priors we furthermore present explicit next-to-leading-order corrections to the mean-field theories, which are valid for general activation functions.

The mean-field theories for the statistics within a layer of the DNN and for the equal-time statistics of the RNN are identical, even if temporally correlated input sequences are supplied to the latter network. The reason is that the mean-field equations (34) form a closed system of equations for this subset of the statistics; they can be solved independently of the correlations across time or layers, respectively. This justifies the ‘annealed approximation’ [39] for RNNs where the couplings are redrawn at each time step—which corresponds to the DNN-prior. It is also compatible with earlier work [52] which compares simulations of networks with tied weights (RNN) to the mean-field theory for untied weights (DNN). Intriguingly, the equivalence of the equal-time statistics implies that the predictive distributions $p(\mathbf{y}^* | \mathbf{x}^*, \mathbf{Y}, \mathbf{X})$ of DNNs and RNNs are identical [53], given the readout is taken only from the final layer or the last time step, respectively.

There are qualitative differences between the mean-field theories for the correlations across time in the RNN and across layers of the DNN: Correlations across layers vanish in the DNN, while the weight sharing in the RNN generally causes non-trivial correlations across time. For point-symmetric activation functions, these correlations also vanish in the RNN if the bias is absent (or uncorrelated across time steps) and the input is provided only in the first step. In general, a linear readout from activations that are taken across different time points or layers, respectively, yields different Gaussian process kernels for the RNN compared to the DNN. Even if the readout is taken at a single layer or time point, respectively, there is an observable difference between DNN and RNN when the fluctuation corrections to the mean field kernels are taken into account: While in RNNs fluctuations are in general correlated across time steps, due to the weight sharing between the time points, fluctuations

are independent across layers for the DNN. As a result, in case of the RNN, the fluctuations at the readout $\Delta_{11}^{(A+1,A+1),(A+1,A+1)}$ depend on the fluctuations between all combinations of time points, whereas for the DNN only within-layer fluctuations from all previous layers influence the result.

Numerically, the convergence of finite-size networks of both architectures to the mean-field theory is generally fast. The RNN converges typically slower than the DNN, at least for long times and correspondingly deep networks. We hypothesize that the temporally correlated activity in the RNN is the cause: The realization of the coupling matrix is the same for all time steps. Also, fluctuations of the activity are coherent over time. Activity and connectivity therefore interact coherently over multiple time steps, so that variations of the connectivity across realizations may cause a corresponding variability of activity. In a DNN, in contrast, both activity and connectivity are uncorrelated across layers, so that variations due to different realizations of the couplings average out over layers. The larger discrepancy between the theoretical prediction and the simulation in case of the RNN as compared to the DNN can also be observed for the next-to-leading-order corrections. Although the form of the corrections differ between RNN and DNN, for the RNN the range of widths that the theory can capture within some given error margin is smaller than the range of validity for the DNN. This implies that overall finite size effects are more relevant in RNNs than they are in DNNs.

Identical mean-field theories in the single-input case and for point-symmetric activation functions were already presented in ref. [40] in the context of a characterization of the space of Boolean functions implemented by randomly coupled DNNs and RNNs. Since our work differs on a conceptual level, the implications of the results differ: In the Bayesian inference picture, the equivalent mean-field theories imply identical performance of the networks for both architectures at large width; for the characterization of computed Boolean functions, the equivalent mean-field theories imply an equivalent set of functions implemented by any two random instances of the two architectures at large width. The conceptual difference leads to further differences on the technical level: The inputs and outputs considered here include analog values and they are presented not only to the first layer or time step, respectively, but also in a sequential manner at subsequent times or layers. Finally, the disorder average plays a subtle but fundamentally different role in the two works: In ref. [40], the disorder average extracts the typical behavior of any single, sufficiently large, instance of a randomly coupled network. In contrast, in the Bayesian framework considered in this manuscript, the disorder average naturally arises from the marginalization of the parameter prior, i.e., one here considers ensembles of random networks.

The analysis of RNNs and DNNs in this manuscript is based on methods from statistical field theory and our results are formulated in that language [43]. It is, however, worth noting that we are actually dealing with multi-variate random variables in n dimensions rather than fields, so that mathematical complications with regard to the latter do not appear here. Moreover, the field-theoretical approach to compute the leading order as a saddle point approximation and the next-to-leading order in n^{-1} from the stability matrix can be connected to the approach of large-deviation theory [54]; exploring this link further is an interesting topic for future research.

There has been previous theoretical work on networks of finite width $n_\ell < \infty$ that is, however, restricted to DNNs. Two different approximation techniques have been employed. The perturbative approach computes corrections where the non-linear terms constitute the expansion parameter; this typically requires analytic activation

functions that can be expanded in low order monomials. The Edgeworth expansion, in contrast, obtains approximations in the strength of the non-Gaussian cumulants as an expansion parameter. Refs. [17, 18, 21, 22, 28] have presented approaches based on perturbation theory, while refs. [19, 23] employed an Edgeworth expansion. These corrections were computed either in the framework of Bayesian inference [17, 19, 23, 28] or gradient-based training [18, 20, 21, 28]. The dynamics of the neural-tangent kernel for deep networks with finite width has been studied in ref. [20]. For specific deep networks of finite width with linear or ReLU activation functions the single-input prior was computed exactly in terms of the Meijer G function in refs. [26, 27].

In this manuscript, we considered the output dimension n_{out} and the depth or number of time-steps A to be fixed. Other works [28, 29] investigated the limit $n \rightarrow \infty$ where A/n is small but finite. Due to the exponential decay of the response functions Δ_{12} , in our setup, this distinction becomes irrelevant as soon as one considers enough layers or time-steps such that the statistics are stationary. In contrast, the output dimension needs to be $O(1)$ in our setup; otherwise, the exponent $\frac{1}{2}\tilde{\mathbf{y}}^T C^{(A+1, A+1)} \tilde{\mathbf{y}}$ in Eq. (27) would not be $O(1)$ and the term would need to be taken into account when deriving the mean-field equation (32) via Eq. (31). Even if the output dimension is $O(1)$, this generally implies a $O(\frac{1}{n})$ correction to the mean-field equations.

While we here focus on the network prior, the recent works by Zavatone-Veth et al. [24] and Naveh and Ringel [25] directly address perturbative effects on the predictive distribution. Zavatone-Veth et al. conjecture a general form of finite width corrections for network observables which result from the linear readout layer and the quadratic loss function. Their expression requires the knowledge of $\text{cov}_{\mathcal{W}}(O, K)$, the covariance of the kernel K and the considered observable O across realizations of the feature map parameters \mathcal{W} . Explicit finite-width corrections are obtained for fully connected and convolutional deep linear networks with and without skip connections. Their computation is perturbative in the non-Gaussian terms and proceeds iteratively, layer by layer. The work by Naveh and Ringel consists of two parts: First, they compute the correction to the mean of the predictive distribution that arises from non-Gaussian cumulants of the process. The correction follows as the solution of a set of self-consistency equations. Second, they compute non-Gaussian corrections perturbatively for shallow fully connected and convolutional feed-forward networks with linear and quadratic activation functions. The general results by Zavatone-Veth et al. and Naveh and Ringel could directly be applied to compute corrections to the mean of the predictive distribution based on the finite-size corrections we have found here, thereby extending their work to nonlinear DNNs and RNNs with arbitrary activation functions.

In a concurrent work, Grosvenor and Jefferson [29] extend the dynamical mean-field theory of recurrent networks in continuous time [31] within the field-theoretical formulation [35, 48] beyond the mean-field limit in order to obtain finite-size corrections for stationary statistics and for the transition to chaos. They proceed with a perturbation expansion around the infinite width mean-field solution, taking into account the nonlinearities approximately via their low-order Taylor monomials and find that the width over the depth is the effective expansion parameter. In contrast to our work, in addition to the different dynamical network equations, they focus on the stationary regime whereas we take the non-stationary propagation of the input through layers or time, respectively, into account.

A further difference between these previous works and the present work is that we present the next-to-leading order correction ($\propto n^{-1}$) in the fluctuation expansion

of the auxiliary fields, as opposed to a perturbation expansion on the level of neuronal fields. We obtain these results in a global manner for all layers or time steps simultaneously, rather than iteratively across layers. Thus, we do not need to truncate the approximation at intermediate layers. Moreover, our approach applies to deep and recurrent fully connected networks, including the full nonlinearity, rather than its polynomial approximation. To our knowledge, our work is the first to derive mean-field and beyond mean-field corrections for DNN and RNN in a unified framework which allows us to discuss the qualitative differences between these two architectures.

Acknowledgments

We would like to thank Bo Li, Alexander Mozeika, and David Saad for bringing their related work to our attention. Furthermore, we would like to thank the anonymous reviewers for helpful comments and suggestions. This work was partially supported by the European Union’s Horizon 2020 research and innovation program under Grant agreement No. 945539 (Human Brain Project SGA3), the Helmholtz Association Initiative and Networking Fund under project number SO-092 (Advanced Computing Architectures, ACA), the German Federal Ministry for Education and Research (BMBF Grant 01IS19077A), and the Excellence Initiative of the German federal and state governments (ERS PF-JARA-SDS005).

6. Appendix

6.1. Unified field theoretical approach for multiple input sequences

Here, we show the derivation of the mean-field equations with more than one input sequence $\{\mathbf{x}_\alpha^{(0)}, \dots, \mathbf{x}_\alpha^{(A)}\}$, the generalization of the derivation presented in the main text. We introduce Greek indices $\alpha \in \{1, \dots, n_D\}$ for the different input vectors that we also call ‘replicas’ in the following. Equations for the single-replicon case in the main text can be obtained by setting $n_D = 1$; the non-sequential input case follows by setting $\mathbf{x}_\alpha^{(a)} = 0$ for $a > 0$ and all α .

6.1.1. Action and auxiliary variables We start from the parameterized likelihood for multiple replicas

$$p(\mathbf{Y} | \mathbf{X}, \boldsymbol{\theta}) = \prod_{\alpha=1}^{n_D} \left\{ \int \mathcal{D}\mathbf{h}_\alpha \delta\left(\mathbf{y}_\alpha - \mathbf{W}^{(\text{out})} \boldsymbol{\phi}_\alpha^{(A)} - \boldsymbol{\xi}^{(A+1)}\right) \right. \\ \times \prod_{a=1}^A \delta\left(\mathbf{h}_\alpha^{(a)} - \mathbf{W}^{(a)} \boldsymbol{\phi}_\alpha^{(a-1)} - \mathbf{W}^{(\text{in},a)} \mathbf{x}_\alpha^{(a)} - \boldsymbol{\xi}^{(a)}\right) \\ \left. \times \delta\left(\mathbf{h}_\alpha^{(0)} - \mathbf{W}^{(\text{in},0)} \mathbf{x}_\alpha^{(0)} - \boldsymbol{\xi}^{(0)}\right) \right\}.$$

Expressing the Dirac distributions as integrals $\delta(x) = \int_{i\mathbb{R}} \frac{d\tilde{x}}{2\pi i} e^{\tilde{x}x}$, we obtain for the network prior $p(\mathbf{Y} | \mathbf{X}) = \int d\boldsymbol{\theta} p(\mathbf{Y} | \mathbf{X}, \boldsymbol{\theta}) p(\boldsymbol{\theta})$ the expression

$$\begin{aligned}
p(\mathbf{Y} | \mathbf{X}) &= \prod_{\alpha=1}^{n_D} \left\{ \int d\tilde{\mathbf{y}}_{\alpha} \int D\mathbf{h}_{\alpha} \int D\tilde{\mathbf{h}}_{\alpha} \right\} e^{\tilde{y}_{i,\alpha} y_{i,\alpha} + \sum_{a=0}^A \tilde{h}_{i,\alpha}^{(a)} h_{i,\alpha}^{(a)}} \\
&\quad \times \langle e^{-\tilde{y}_{i,\alpha} W_{ij}^{(\text{out})} \phi_{j,\alpha}^{(A)}} \rangle_{\mathbf{W}^{(\text{out})}} \langle e^{-\sum_{a=1}^A \tilde{h}_{i,\alpha}^{(a)} W_{ij}^{(a)} \phi_{j,\alpha}^{(a-1)}} \rangle_{\{\mathbf{W}^{(a)}\}} \\
&\quad \times \langle e^{-\sum_{a=0}^A \tilde{h}_{i,\alpha}^{(a)} W_{ij}^{(\text{in},a)} x_{j,\alpha}^{(a)}} \rangle_{\{\mathbf{W}^{(\text{in},a)}\}} \\
&\quad \times \langle e^{-\sum_{\alpha=1}^{n_D} \sum_{a=0}^A \tilde{h}_{i,\alpha}^{(a)} \xi_i^{(a)} - \sum_{\alpha=1}^{n_D} \tilde{y}_{i,\alpha} \xi_i^{(A+1)}} \rangle_{\{\boldsymbol{\xi}^{(a)}\}}. \quad (45)
\end{aligned}$$

Here, and throughout this section, we use an implicit summation convention for lower indices that appear twice in the exponent, e.g., $\tilde{y}_{i,\alpha} y_{i,\alpha} \equiv \sum_{\alpha=1}^{n_D} \sum_{i=1}^{n_{\text{out}}} \tilde{y}_{i,\alpha} y_{i,\alpha}$, but write the sum over time steps explicitly to avoid ambiguities in their limits. Note that for the DNN, the number of neurons per layer can differ such that formally the upper limits of the implicit sums over neuron indices i or j depends on the layer index a . We also used the independence of the different weight matrices and biases to obtain factorizing expectation values in Eq. (45).

In the following, we compute these expectation values separately, starting with the output weights and biases. These are independent across neurons and we obtain

$$\begin{aligned}
\left\langle \exp \left(- \sum_{\alpha=1}^{n_D} \tilde{y}_{i,\alpha} \xi_i^{(A+1)} \right) \right\rangle_{\boldsymbol{\xi}^{(A+1)}} &= \exp \left(\frac{\sigma_{A+1}^2}{2} \sum_{\alpha,\beta=1}^{n_D} \tilde{y}_{i,\alpha} \tilde{y}_{i,\beta} \right), \\
\left\langle \exp \left(- \tilde{y}_{i,\alpha} W_{ij}^{(\text{out})} \phi_{j,\alpha}^{(A)} \right) \right\rangle_{\mathbf{W}^{(\text{out})}} &= \exp \left(\frac{g_{A+1}^2}{2n_A} \tilde{y}_{i,\alpha} \phi_{j,\alpha}^{(A)} \phi_{j,\beta}^{(A)} \tilde{y}_{i,\beta} \right).
\end{aligned}$$

Now, we calculate the respective averages for the RNN and DNN separately. For a RNN, the weight sharing $\mathbf{W}^{(a)} \equiv \mathbf{W}$ across time steps a leads to a double sum $\sum_{a,b}$ appearing in the average over the recurrent part

$$\begin{aligned}
&\left\langle \exp \left(- \sum_{a=1}^A \tilde{h}_{i,\alpha}^{(a)} W_{ij} \phi_{j,\alpha}^{(a-1)} \right) \right\rangle_{\mathbf{W}} \\
&= \exp \left(\frac{1}{2} \sum_{a,b=1}^A \frac{g_a^2}{n} \tilde{h}_{i,\alpha}^{(a)} \phi_{j,\alpha}^{(a-1)} \phi_{j,\beta}^{(b-1)} \tilde{h}_{i,\beta}^{(b)} \right), \quad \text{RNN.}
\end{aligned}$$

In contrast, for a DNN, the analogous calculation leads to a single sum \sum_a

$$\begin{aligned}
&\left\langle \exp \left(- \sum_{a=1}^A \tilde{h}_{i,\alpha}^{(a)} W_{ij}^{(a)} \phi_{j,\alpha}^{(a-1)} \right) \right\rangle_{\{\mathbf{W}^{(a)}\}} \\
&= \prod_{a=1}^A \left\langle \exp \left(- \tilde{h}_{i,\alpha}^{(a)} W_{ij}^{(a)} \phi_{j,\alpha}^{(a-1)} \right) \right\rangle_{\mathbf{W}^{(a)}} \\
&= \exp \left(\frac{1}{2} \sum_{a=1}^A \frac{g_a^2}{n_{a-1}} \tilde{h}_{i,\alpha}^{(a)} \phi_{j,\alpha}^{(a-1)} \phi_{j,\beta}^{(a-1)} \tilde{h}_{i,\beta}^{(a)} \right), \quad \text{DNN.}
\end{aligned}$$

The calculation for the inputs and biases is analogous; for the RNN it yields

$$\left\langle \exp \left(- \sum_{a=0}^A \sum_{\alpha=1}^{n_D} \tilde{h}_{i,\alpha}^{(a)} \xi_i^{(a)} \right) \right\rangle_{\boldsymbol{\xi}}$$

$$\begin{aligned}
&= \exp \left(\frac{\sigma^2}{2} \sum_{a,b=0}^A \sum_{\alpha,\beta=1}^{n_D} \tilde{h}_{i,\alpha}^{(a)} \tilde{h}_{i,\beta}^{(b)} \right), \quad \text{RNN}, \\
&\left\langle \exp \left(- \sum_{a=0}^A \tilde{h}_{i,\alpha}^{(a)} W_{ij}^{(\text{in})} x_{j,\alpha}^{(a)} \right) \right\rangle_{\mathbf{W}^{(\text{in})}} \\
&= \exp \left(\frac{1}{2} \sum_{a,b=0}^A \frac{g_0^2}{n_{\text{in}}} \tilde{h}_{i,\alpha}^{(a)} x_{j,\alpha}^{(a)} x_{j,\beta}^{(b)} \tilde{h}_{i,\beta}^{(b)} \right), \quad \text{RNN}.
\end{aligned}$$

For the DNN, we get

$$\begin{aligned}
&\left\langle \exp \left(- \sum_{a=0}^A \sum_{\alpha=1}^{n_D} \tilde{h}_{i,\alpha}^{(a)} \xi_i^{(a)} \right) \right\rangle_{\{\xi^{(a)}\}} \\
&= \prod_{a=0}^A \left\langle \exp \left(- \sum_{\alpha=1}^{n_D} \tilde{h}_{i,\alpha}^{(a)} \xi_i^{(a)} \right) \right\rangle_{\xi^{(a)}} \\
&= \exp \left(\frac{1}{2} \sum_{a=0}^A \sigma_a^2 \sum_{\alpha,\beta=1}^{n_D} \tilde{h}_{i,\alpha}^{(a)} \tilde{h}_{i,\beta}^{(a)} \right), \quad \text{DNN}, \\
&\left\langle \exp \left(- \sum_{a=0}^A \tilde{h}_{i,\alpha}^{(a)} W_{ij}^{(\text{in},a)} x_{j,\alpha}^{(a)} \right) \right\rangle_{\{\mathbf{W}^{(\text{in},a)}\}} \\
&= \prod_{a=0}^A \left\langle \exp \left(- \tilde{h}_{i,\alpha}^{(a)} W_{ij}^{(\text{in},a)} x_{j,\alpha}^{(a)} \right) \right\rangle_{\mathbf{W}^{(\text{in},a)}} \\
&= \exp \left(\frac{1}{2} \sum_{a=0}^A \frac{g_0^2}{n_{\text{in}}} \tilde{h}_{i,\alpha}^{(a)} x_{j,\alpha}^{(a)} x_{j,\beta}^{(a)} \tilde{h}_{i,\beta}^{(a)} \right), \quad \text{DNN}.
\end{aligned}$$

For the RNN, the replicas as well as the time steps are coupled by the products $\phi_{j,\alpha}^{(a-1)} \phi_{j,\beta}^{(b-1)}$ and $x_{j,\alpha}^{(a)} x_{j,\beta}^{(b)}$, while for the DNN only products of terms within the same layer occur, $\phi_{j,\alpha}^{(a-1)} \phi_{j,\beta}^{(a-1)}$ and $x_{j,\alpha}^{(a)} x_{j,\beta}^{(a)}$. As we will show below, this leads to different layers in the DNN being uncorrelated, while different time steps in the RNN are correlated.

The products of nonlinearly transformed pre-activations $\phi_{i,\alpha}^{(a)} \equiv \phi(h_{i,\alpha}^{(a)})$ render the integrations in Eq. (45) analytically non-solvable. To find a suitable approximation, we insert auxiliary variables in time (a, b) and in replica space (α, β) , which account for the replica and time-step coupling. Introducing these, the system decouples in the neuron indices i . We combine RNN and DNN by defining the auxiliary variables

$$\begin{aligned}
C_{\alpha,\beta}^{(a,b)} &= M_{a,b} \left[\sigma_a^2 + \frac{g_a^2}{n_{a-1}} \mathbb{1}_{a \geq 1, b \geq 1} \phi_{i,\alpha}^{(a-1)} \phi_{i,\beta}^{(b-1)} \right. \\
&\quad \left. + \frac{g_0^2}{n_{\text{in}}} \mathbb{1}_{a \leq A, b \leq A} x_{i,\alpha}^{(a)} x_{i,\beta}^{(b)} \right] \quad (46)
\end{aligned}$$

for $0 \leq a, b \leq A+1$ with $M_{a,b}$ defined in Eq. (25), $g_a = g$ for $1 \leq a \leq A$ in RNN, and $n_{-1} \equiv n_{\text{in}}$. The indicator functions $\mathbb{1}_{a \geq 1, b \geq 1}$ and $\mathbb{1}_{a \leq A, b \leq A}$ ensure that the respective

terms vanish when they are not present, e.g., the recurrent term $\phi_{i,\alpha}^{(a-1)} M_{a,b} \phi_{i,\beta}^{(b-1)}$ in the first step $a = b = 0$. As above, there is an implicit sum over the neuron indices i on the right hand side.

We introduce these auxiliary variables by means of Dirac distributions expressed as Fourier integrals

$$\begin{aligned} \delta[\text{Eq. (46)}] &= \prod_{\alpha,\beta=1}^{n_D} \prod_{a,b=0}^{A+1} \left\{ n_{a-1} \int_{i\mathbb{R}} \frac{d\tilde{C}_{\alpha,\beta}^{(a,b)}}{2\pi i} \right\} \\ &\times \exp \left(- \sum_{a,b=0}^{A+1} n_{a-1} \tilde{C}_{\alpha,\beta}^{(a,b)} (C_{\alpha,\beta}^{(a,b)} - \sigma_a^2 M_{a,b} J_{\alpha,\beta}) \right) \\ &\times \exp \left(\sum_{a,b=1}^{A+1} \tilde{C}_{\alpha,\beta}^{(a,b)} g_a^2 \phi_{i,\alpha}^{(a-1)} M_{a,b} \phi_{i,\beta}^{(b-1)} \right) \\ &\times \exp \left(\sum_{a,b=0}^A n_{a-1} \tilde{C}_{\alpha,\beta}^{(a,b)} \frac{g_0^2}{n_{\text{in}}} x_{i,\alpha}^{(a)} M_{a,b} x_{i,\beta}^{(b)} \right), \end{aligned} \quad (47)$$

where we inserted $J_{\alpha,\beta} = 1$ for all α and β to imply the summation over α, β that accounts for the common biases across replicas. Used in the integrand of Eq. (45), this leads to

$$\begin{aligned} p(\mathbf{Y} | \mathbf{X}) &= \prod_{\alpha=1}^{n_D} \left\{ \int d\tilde{\mathbf{y}}_\alpha \int D\mathbf{h}_\alpha \int D\tilde{\mathbf{h}}_\alpha \right\} \prod_{\alpha,\beta=1}^{n_D} \left\{ \int D\tilde{C}_{\alpha,\beta} \int DC_{\alpha,\beta} \right\} \\ &\times \exp \left(\tilde{y}_{i,\alpha} y_{i,\alpha} + \frac{1}{2} \tilde{y}_{i,\alpha} C_{\alpha,\beta}^{(A+1,A+1)} \tilde{y}_{i,\beta} \right) \\ &\times \exp \left(\sum_{a=0}^A \tilde{h}_{i,\alpha}^{(a)} h_{i,\alpha}^{(a)} + \sum_{a,b=0}^A \frac{1}{2} \tilde{h}_{i,\alpha}^{(a)} C_{\alpha,\beta}^{(a,b)} \tilde{h}_{i,\beta}^{(b)} \right) \\ &\times \exp \left(- \sum_{a,b=0}^{A+1} n_{a-1} \tilde{C}_{\alpha,\beta}^{(a,b)} (C_{\alpha,\beta}^{(a,b)} - \sigma_a^2 M_{a,b} J_{\alpha,\beta}) \right) \\ &\times \exp \left(\sum_{a,b=1}^{A+1} \tilde{C}_{\alpha,\beta}^{(a,b)} g_a^2 \phi_{i,\alpha}^{(a-1)} M_{a,b} \phi_{i,\beta}^{(b-1)} \right) \\ &\times \exp \left(\sum_{a,b=0}^A n_{a-1} \tilde{C}_{\alpha,\beta}^{(a,b)} \frac{g_0^2}{n_{\text{in}}} x_{i,\alpha}^{(a)} M_{a,b} x_{i,\beta}^{(b)} \right) \end{aligned} \quad (48)$$

with $DC_{\alpha,\beta} = \prod_{a,b=0}^{A+1} dC_{\alpha,\beta}^{(a,b)}$, $D\tilde{C}_{\alpha,\beta} = \prod_{a,b=0}^{A+1} \frac{n_{a-1} d\tilde{C}_{\alpha,\beta}^{(a,b)}}{2\pi i}$.

We see in Eq. (48) that there are no auxiliary variables $C_{\alpha,\beta}^{(a,b)}$ that couple the output layer ($a = A + 1$, second line) with variables $\mathbf{h}_\alpha^{(a)}, \tilde{\mathbf{h}}_\alpha^{(a)}$ in the rest of the network ($0 \leq a \leq A$). This is a consequence of the independence of the priors on the associated weights. We further see in Eq. (48) that no products of variables with different neuron indices appear. The exponential thus factorizes into n_a identical terms for each a . Rearranging the integrations, we obtain

$$p(\mathbf{Y} | \mathbf{X}) = \prod_{\alpha=1}^{n_D} \left\{ \int d\tilde{\mathbf{y}}_{\alpha} \right\} e^{\tilde{\mathbf{y}}_{i,\alpha} y_{i,\alpha}} \left\langle e^{\frac{1}{2} \tilde{\mathbf{y}}_{i,\alpha} C_{\alpha,\beta}^{(A+1,A+1)} \tilde{\mathbf{y}}_{i,\beta}} \right\rangle_{\tilde{C},C} \quad (49)$$

where the expectation value is computed with respect to the action

$$\mathcal{S}_{\text{aux}}(C, \tilde{C}) = -n \sum_{a,b=0}^{A+1} \nu_{a-1} \tilde{C}_{\alpha,\beta}^{(a,b)} C_{\alpha,\beta}^{(a,b)} + n \mathcal{W}_{\text{aux}}(\tilde{C} | C) \quad (50)$$

of the auxiliary variables $\tilde{C}_{\alpha,\beta}^{(a,b)}, C_{\alpha,\beta}^{(a,b)}$. This action comprises the nontrivial part of the dynamics of the network in the cumulant generating functional

$$\begin{aligned} \mathcal{W}_{\text{aux}}(\tilde{C} | C) &= \frac{1}{n} \ln \left\langle e^{\sum_{a,b=1}^{A+1} \tilde{C}_{\alpha\beta}^{(a,b)} g_a^2 \phi_{i,\alpha}^{(a-1)} M_{a,b} \phi_{i,\beta}^{(b-1)}} \right\rangle_{\{h_{i,\alpha}^{(a)}\}} \\ &\quad + \sum_{a,b=0}^A \nu_{a-1} \tilde{C}_{\alpha,\beta}^{(a,b)} \frac{g_0^2}{n_{\text{in}}} x_{i,\alpha}^{(a)} M_{a,b} x_{i,\beta}^{(b)} \\ &\quad + \sum_{a,b=0}^{A+1} \nu_{a-1} \tilde{C}_{\alpha,\beta}^{(a,a)} \sigma_a^2 M_{a,b} J_{\alpha,\beta} \end{aligned} \quad (51)$$

where $\{h_{i,\alpha}^{(a)}\}$ describes the Gaussian statistics of a single pre-activation $h_{i,\alpha}^{(a)}$ with covariance matrix $\langle h_{i,\alpha}^{(a)} h_{i,\beta}^{(b)} \rangle = C_{\alpha,\beta}^{(a,b)} \delta_{i,j}$ across neurons i, j , time steps or layers a, b , and inputs α, β . Here $\nu_a = n_a/n$ denotes the relative layer sizes in the DNN.

To show that

$$\frac{1}{n} \ln \left\langle e^{\sum_{a,b=1}^{A+1} \tilde{C}_{\alpha\beta}^{(a,b)} g_a^2 \phi_{i,\alpha}^{(a-1)} M_{a,b} \phi_{i,\beta}^{(b-1)}} \right\rangle_{\{h_{i,\alpha}^{(a)}\}} = O(1) \quad (52)$$

and thus $\mathcal{W}_{\text{aux}}(\tilde{C} | C) = O(1)$, i.e., that $\mathcal{W}_{\text{aux}}(\tilde{C} | C)$ does not scale with n , we consider RNN and DNN separately. For the RNN, the result immediately follows because the neurons are uncorrelated, $\langle h_{i,\alpha}^{(a)} h_{i,\beta}^{(b)} \rangle = C_{\alpha,\beta}^{(a,b)} \delta_{i,j}$, which factorizes the expectations and leads to a sum over n identical terms:

$$\begin{aligned} &\frac{1}{n} \ln \left\langle e^{\sum_{a,b=1}^{A+1} \tilde{C}_{\alpha\beta}^{(a,b)} g_a^2 \phi_{i,\alpha}^{(a-1)} \phi_{i,\beta}^{(b-1)}} \right\rangle_{\{h_{i,\alpha}^{(a)}\}} \\ &= \ln \left\langle e^{\sum_{a,b=1}^{A+1} \tilde{C}_{\alpha\beta}^{(a,b)} g_a^2 \phi_{\alpha}^{(a-1)} \phi_{\beta}^{(b-1)}} \right\rangle_{\{h_{\alpha}^{(a)}\}}. \end{aligned}$$

For the DNN, one first notices that, by definition, $C_{\alpha,\beta}^{(a,b)} = 0$ for $a \neq b$, so different layers decouple in Eq. (51). Formally this can be seen by solving the integrals over the corresponding variables $\tilde{C}_{\alpha,\beta}^{(a,b)}$ with $a \neq b$. This factorization allows us to study each layer separately and decouple the n_a neurons:

$$\begin{aligned} &\frac{1}{n} \ln \left\langle e^{\sum_{a=1}^{A+1} \tilde{C}_{\alpha\beta}^{(a,a)} g_a^2 \phi_{i,\alpha}^{(a-1)} \phi_{i,\beta}^{(a-1)}} \right\rangle_{\{h_{i,\alpha}^{(a)}\}} \\ &= \sum_{a=1}^{A+1} \nu_{a-1} \ln \left\langle e^{\tilde{C}_{\alpha\beta}^{(a,a)} g_a^2 \phi_{\alpha}^{(a-1)} \phi_{\beta}^{(a-1)}} \right\rangle_{\{h_{\alpha}^{(a)}\}}. \end{aligned}$$

Consequently, for both architectures Eq. (52) holds and $\mathcal{W}_{\text{aux}}(\tilde{C} | C) = O(1)$.

6.1.2. Saddle-point approximation The action \mathcal{S}_{aux} in the auxiliary fields scales with the number of neurons n . In the limit $n \rightarrow \infty$, a saddle-point approximation of the integrals over \tilde{C} and C appearing in the expectation value in Eq. (49) becomes exact. The saddle points are determined by the stationary points of the action \mathcal{S}_{aux} as $\frac{\partial}{\partial \tilde{C}_{\alpha,\beta}^{(a,b)}} \mathcal{S}_{\text{aux}}(C, \tilde{C}) \stackrel{!}{=} 0$ and $\frac{\partial}{\partial C_{\alpha,\beta}^{(a,b)}} \mathcal{S}_{\text{aux}}(C, \tilde{C}) \stackrel{!}{=} 0$, leading to

$$\overline{\tilde{C}}_{\alpha\beta}^{(a,b)} = 0, \quad (53)$$

$$\overline{C}_{\alpha\beta}^{(a,b)} = M_{a,b} \left[\sigma_a^2 + \frac{g_0^2}{n_{\text{in}}} \mathbb{1}_{a \leq A, b \leq A} x_{i,\alpha}^{(a)} x_{i,\beta}^{(b)} + g_a^2 \mathbb{1}_{a \geq 1, b \geq 1} \langle \phi(h_\alpha^{(a-1)}) \phi(h_\beta^{(b-1)}) \rangle_{\{h_\alpha^{(a)}\} \sim \mathcal{N}(0, \overline{C})} \right] \quad (54)$$

with indices $a, b \in \{0, \dots, A+1\}$. The saddle point $\overline{\tilde{C}}_{\alpha\beta}^{(a,b)} = 0$ is a self-consistent solution because $W_{\text{aux}}(0 | C) \equiv 0$, which is in particular independent of C , so that $\partial W_{\text{aux}}(0 | C) / \partial C_{\alpha,\beta}^{(a,b)} \equiv 0$.

To evaluate the expectation value on the r.h.s. of Eq. (54), we only need the sub-tensors of \overline{C} formed by the indices that explicitly appear in the expectation due to the marginalization property of the Gaussian. In particular, this means the saddle point equations can be solved iteratively starting from $a = 0$, which requires the starting values $\overline{C}_{\alpha\beta}^{(0,a)} = \overline{C}_{\alpha\beta}^{(a,0)} = M_{a,0} \left[\sigma_0^2 + \frac{g_0^2}{n_{\text{in}}} \sum_{j=1}^{n_{\text{in}}} x_{j,\alpha}^{(a)} x_{j,\beta}^{(0)} \right]$ for the recursion.

After the saddle-point approximation, the conditional probability Eq. (49) simplifies to the factorized Gaussian

$$p(\mathbf{Y} | \mathbf{X}) = \prod_{i=1}^{n_{A+1}} p(\mathbf{y}_i | \mathbf{X}),$$

$$p(\mathbf{y}_i | \mathbf{X}) = \mathcal{N}(0, \overline{C}^{(A+1, A+1)}),$$

with covariance matrix $\langle y_{i,\alpha} y_{i,\beta} \rangle = \overline{C}_{\alpha,\beta}^{(A+1, A+1)}$ across inputs α, β that is determined recursively by Eq. (54), starting from the input covariance $\overline{C}_{\alpha\beta}^{(0,0)} = \sigma_0^2 + \frac{g_0^2}{n_{\text{in}}} \sum_{j=1}^{n_{\text{in}}} x_{j,\alpha}^{(0)} x_{j,\beta}^{(0)}$. The diagonal elements $\overline{C}_{\alpha,\beta}^{(A+1, A+1)}$ thus only depends on the equal-time overlaps $\sum_{i=1}^{n_{\text{in}}} x_{i,\alpha}^{(a)} x_{i,\beta}^{(a)}$ of the inputs with $0 \leq a \leq A$.

6.2. Finite-size instability of RNNs

In the main text Figure 1, the mean-field theory is compared to network simulations with hidden layer width $n = 2000$ and a ReLU nonlinearity for fixed hyperparameters $g^2 = 1.6$, $\sigma^2 = 0.2$. Although this appears to be quite wide already, for the RNN the statistics of the activity in individual networks strongly varies across realizations of weights. The frequency of deviating realizations increases as one approaches $g^2 \rightarrow 2$, the instability threshold above which $\overline{C}^{(a,a)}$ diverges with growing a for the ReLU nonlinearity. The instability threshold can be obtained from the MFT solution for a single replicon and $a = b$, Eq. (57): The theory predicts that $g^2 > 2$ will lead to exponential increase of the activity, while $g^2 < 2$ results in finite (but possibly very strong) activity. Beyond this threshold, trajectories of individual neurons diverge towards $\pm\infty$ over time. At finite width and $g^2 < 2$, the activity is typically stable. But for g^2 sufficiently close to 2, the closeness of the instability point is visible in the

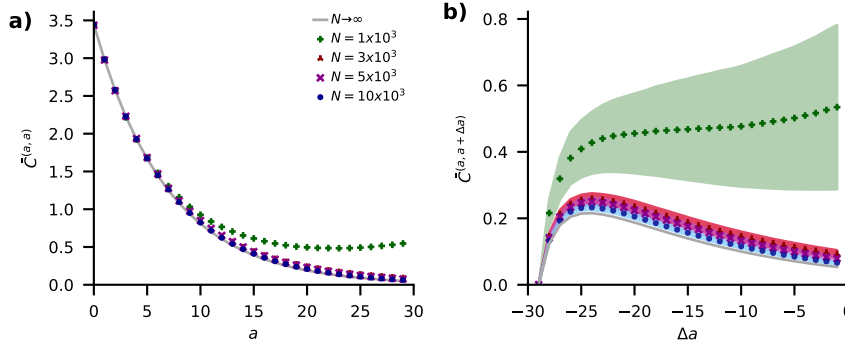


Figure 4. Mean-field theory of the RNN compared to simulation. a Average variance in mean-field theory $\bar{C}^{(a,a)}$ (solid gray curve) and estimate $\frac{1}{n} \sum_i h_i^{(a)} h_i^{(a)}$ from simulation, averaged over 100 realizations of networks with different widths (symbols, see legend). **b** Average cross-covariance in mean-field-theory $\bar{C}^{(a,a+\Delta a)}$ and estimate $\frac{1}{n} \sum_i h_i^{(a)} h_i^{(a+\Delta a)}$ from simulation, averaged over 100 network realizations (mean shown as symbols, same symbol code as in panel a; standard error of the mean shown as tube), as a function of the temporal distance Δa to the hidden layer $a = 30$. Mean-field theory (gray curve). Other parameters: $g^2 = 1.73$, $\sigma^2 = 0$, layer widths $n_a \in \{1, 3, 5, 10\} \cdot 10^3$, $A = 30$ hidden layers, ReLU activation $\phi(x) = \max(0, x)$ and Gaussian input $\mathbf{x} \stackrel{\text{i.i.d.}}{\sim} \mathcal{N}(1, 1)$ with $\dim(\mathbf{x}) = 10^5$.

system. This is observable as a spread of individual neurons' trajectories, each hovering about a non-zero set point. This observation corresponds to a static contribution (independent of Δa) to the time-lagged correlation function, as shown in Figure 4b. The reason for this instability to only occur in the RNN is the coherent interplay of the activity with the connectivity across time: Since the connectivity is identical across all time steps, fluctuations of the activity can be amplified coherently across multiple time steps. Likewise, deviations of the variances $C^{(a,a)}$ are observable in this case (Figure 4a). The effect is suppressed as the network size increases; the mean-field theory then becomes accurate also for values of g^2 close to 2 (Figure 4a,b).

6.3. Mean-field theory for error function nonlinearity

While we calculated and discussed the temporal structure of the mean-field kernel for the ReLU activation function in the main text, we here focus on the odd activation function $\phi(x) = \text{erf}(\sqrt{\pi}x/2)$ (the scaling ensures $\phi'(0) = 1$) and the single input case. For the auto-correlation (Figure 5 panel a for uncorrelated bias and c for static bias), we see good agreement with the theory, similar to $\phi = \text{ReLU}$ case in Figure 1 in the main text. The temporal or layer-wise correlations are shown in panels b and d. As discussed in Section 4.1, neither temporal nor layer-wise correlations can arise in the uncorrelated bias case: For the DNN this is clear for any activation function due to the independently drawn weights, but also in the RNN case correlations vanish because erf is an odd function. However, if temporal correlations are induced via a static bias, as in panel d, these can be strengthened by the weight sharing. In DNNs on the other hand, all correlations can be accounted to the static bias applied in each layer. Note that the fluctuations are smaller for $\phi = \text{erf}$ than for $\phi = \text{ReLU}$ (compare Figure 1 and Figure 5).

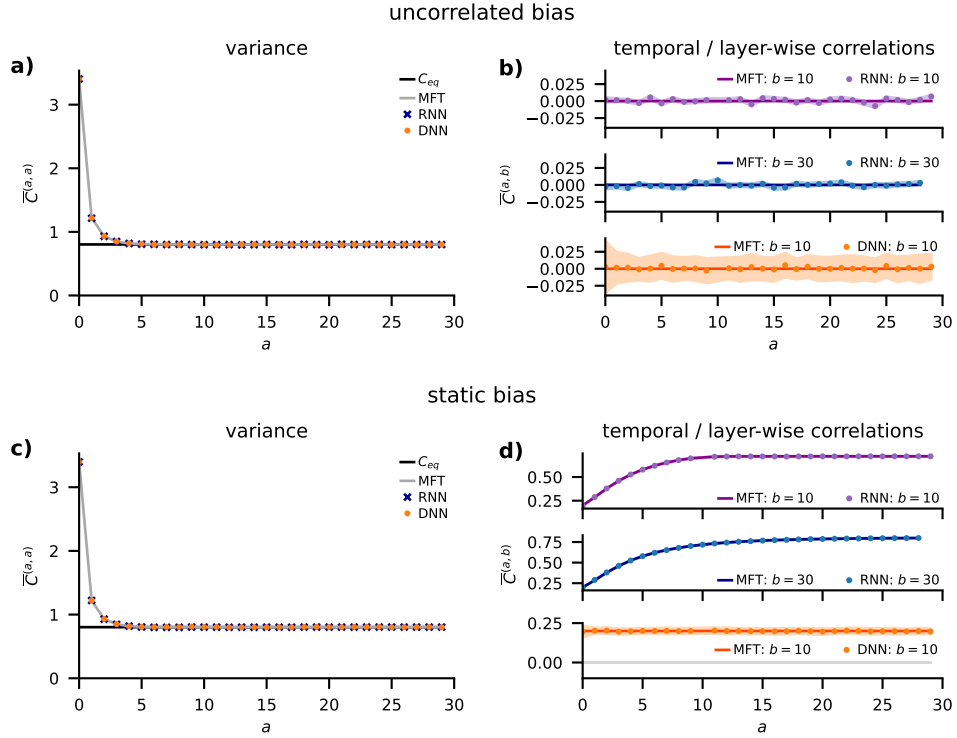


Figure 5. Mean-field theory for DNN and RNN with a single input. **a)** Average variance in mean-field theory $\overline{C}^{(a,a)}$ (Eq. (32); solid gray curve) and estimate $\frac{1}{n_a} \sum_i h_i^{(a)} h_i^{(a)}$ from simulation, averaged over 100 realizations of networks, for biases that are uncorrelated across time/layers (blue crosses RNN; orange dots DNN). **b)** Cross-covariance $\overline{C}^{(a,b)}$ as a function of the hidden layer index a for fixed $b \in \{10, 30\}$ and uncorrelated biases. RNN: Mean-field theory (solid dark blue and dark magenta). Mean (blue / purple dots) and standard error of the mean (light blue / light purple tube) of $\frac{1}{n_a} \sum_i h_i^{(a)} h_i^{(b)}$ estimated from simulation of 100 network realizations. DNN: Mean (orange dots) and standard error of the mean of $\frac{1}{n_a} \sum_i h_i^{(a)} h_i^{(b)}$ estimated from simulation of 100 network realizations. Other parameters $g_0^2 = g^2 = 1.6$, $\sigma^2 = 0.2$, finite layer width $n_a = 2000$, $A = 30$ hidden layers, activation $\phi(x) = \text{erf}(\sqrt{\pi}x/2)$ and Gaussian inputs $\mathbf{x} \stackrel{\text{i.i.d.}}{\sim} \mathcal{N}(1, 1)$ with $n_{\text{in}} = 10^5$. **c)** Same as a) but for biases that are static across time/layers. **d)** Same as b) but for the static bias case.

6.4. Details about numerical experiments

For all experiments, we used NumPy [55] and SciPy [56] which are both released under a BSD-3-Clause License. Computations were performed on a CPU cluster. More precisely, the requirements for the experiments are:

- Figure 1 (main): 1h on a single core laptop.
- Figure 2 (main): 50h on a single node with 24 cores of a CPU cluster for each of panel a and c, and 2h on a single node with 24 cores of the CPU cluster for each of panel b and d.

- Figure 3 (main): 1h on a single core laptop.
- Figure 4 (appendix): 1.5h on a single core laptop.
- Figure 5 (appendix): 1h on a single core laptop.

The code used to produce the figures is stored in a Zenodo archive with the DOI 10.5281/zenodo.5747219.

To solve the mean field theory for a given activation function $\phi(x)$ one needs to calculate the expectation values in Eq. (32), or more general in Eq. (34). Here we choose the ReLU activation $\phi(x) = \max(0, x)$ as shown in [51]:

$$\langle \phi(x)\phi(y) \rangle_{x, y \sim \mathcal{N}(0, C)} = \frac{1}{2\pi} \nu (\sin \theta + (\pi - \theta) \cos \theta), \quad (55)$$

where

$$\begin{aligned} \nu &= \sqrt{C_{xx}C_{yy}}, \\ \theta &= \cos^{-1} \left(\frac{C_{xy}}{\nu} \right). \end{aligned}$$

Inserting this into the MFT equations for multiple replicas (34) results in

$$\begin{aligned} \overline{C}_{\alpha\beta}^{(a,b)} &= M_{a,b} \left[\sigma_a^2 + \mathbb{1}_{a \geq 1, b \geq 1} \frac{g_a^2}{2\pi} \nu_{\alpha\beta}^{(a,b)} (\sin \theta_{\alpha\beta}^{(a,b)} + (\pi - \theta_{\alpha\beta}^{(a,b)}) \cos \theta_{\alpha\beta}^{(a,b)}) \right. \\ &\quad \left. + \mathbb{1}_{a \leq A, b \leq A} \frac{g_0^2}{n_{\text{in}}} \mathbf{x}_\alpha^{(a)\text{T}} \mathbf{x}_\beta^{(b)} \right], \end{aligned} \quad (56)$$

where

$$\begin{aligned} \nu_{\alpha\beta}^{(a,b)} &= \sqrt{\overline{C}_{\alpha\alpha}^{(a-1, a-1)} \overline{C}_{\beta\beta}^{(b-1, b-1)}}, \\ \theta_{\alpha\beta}^{(a,b)} &= \cos^{-1} \left(\frac{\overline{C}_{\alpha\beta}^{(a-1, b-1)}}{\nu_{\alpha\beta}^{(a,b)}} \right). \end{aligned}$$

The special case $a = b$, $\alpha = \beta$, and vanishing external input yields

$$\overline{C}^{(a,a)} = \sigma_a^2 + \frac{g_a^2}{2} \overline{C}^{(a-1, a-1)}. \quad (57)$$

For time or layer independent $g_a \equiv g$ and $\sigma_a \equiv \sigma$, the activity thus increases exponentially in time or over layers for $g^2 > 2$ and converges towards an equilibrium value $C^{(\infty)} = \frac{\sigma^2}{1-g^2/2}$ for $g^2 < 2$.

For the results based on $\phi(x) = \text{erf}(\sqrt{\pi}x/2)$ shown in Appendix 6.3, we used [57, 58]

$$\langle \phi(x)\phi(y) \rangle_{x, y \sim \mathcal{N}(0, C)} = \frac{2}{\pi} \arcsin \left(\frac{\frac{\pi}{2} C_{xy}}{\sqrt{1 + \frac{\pi}{2} C_{xx}} \sqrt{1 + \frac{\pi}{2} C_{yy}}} \right).$$

Importantly, the r.h.s. vanishes for uncorrelated inputs with $C_{xy} = 0$.

6.5. Next-to-leading-order corrections

Here, we consider the case of a single input in the initial layer. In this case, the action for the auxiliary variables $\mathcal{S}_{\text{aux}}(C, \tilde{C})$ is given by Eq. (28) together with $\mathcal{W}_{\text{aux}}^{\text{DNN}}(\tilde{C} | C)$

from Eq. (29) for DNNs and $\mathcal{W}_{\text{aux}}^{\text{RNN}}(\tilde{C}|C)$ from Eq. (30) for RNNs. To compute finite-size corrections, we need so compute the Hessian of $\mathcal{S}_{\text{aux}}(C, \tilde{C})$, which is

$$\begin{aligned} \mathcal{S}_{\text{aux}}^{(a,b),(c,d)} &= \begin{pmatrix} \mathcal{S}_{\text{aux},11}^{(a,b),(c,d)} & \mathcal{S}_{\text{aux},12}^{(a,b),(c,d)} \\ \mathcal{S}_{\text{aux},21}^{(a,b),(c,d)} & \mathcal{S}_{\text{aux},22}^{(a,b),(c,d)} \end{pmatrix} \\ &= \begin{pmatrix} 0 & \frac{\partial^2 \mathcal{S}_{\text{aux}}}{\partial C^{(a,b)} \partial \tilde{C}^{(c,d)}} \\ \frac{\partial^2 \mathcal{S}_{\text{aux}}}{\partial \tilde{C}^{(a,b)} \partial C^{(c,d)}} & \frac{\partial^2 \mathcal{S}_{\text{aux}}}{\partial \tilde{C}^{(a,b)} \partial \tilde{C}^{(c,d)}} \end{pmatrix}, \end{aligned} \quad (58)$$

where we used that due to the normalization of $\mathcal{N}(0, C)$ to one, which is in particular independent of C , we have $\partial \mathcal{W}_{\text{aux}} / \partial C^{(a,b)} = 0$ for $\tilde{C} = 0$, so also $\partial^2 \mathcal{S}_{\text{aux}} / \partial C^{(a,b)} \partial C^{(c,d)} = 0$. Note that we here evaluate the fluctuations around the saddle-point where $\overline{\tilde{C}}^{(a,b)} = 0$ and $\overline{C}^{(a,b)}$ is given by Eq. (32); to simplify the notation we drop the overline throughout this subsection. To proceed, we separate the derivation for DNN and RNN due to the difference between $\mathcal{W}_{\text{aux}}^{\text{DNN}}(\tilde{C}|C)$ and $\mathcal{W}_{\text{aux}}^{\text{RNN}}(\tilde{C}|C)$.

6.5.1. DNN First, we focus on the DNN. The off-diagonal elements of the Hessian are

$$\frac{\partial^2 \mathcal{S}_{\text{aux}}}{\partial C^{(a,b)} \partial \tilde{C}^{(c,d)}} = -n \nu_{a-1} \delta_{(a,b),(c,d)} + n \delta_{c,d} \nu_{c-1} g_c^2 \frac{\partial \langle \phi^{(c-1)} \phi^{(c-1)} \rangle}{\partial C^{(a,b)}},$$

where $\delta_{(a,b),(c,d)} = 1$ if $a = c$ and $b = d$ and $\delta_{(a,b),(c,d)} = 0$ otherwise. The derivative in the second term is the linear response of the expectation value $\langle \phi^{(c-1)} \phi^{(c-1)} \rangle$ with regard to changes of $C^{(a,b)}$. Since the former only depends on the statistics of $h^{(c-1)}$ and thus on $C^{(c-1,c-1)}$, we obtain

$$\frac{\partial \langle \phi^{(c-1)} \phi^{(c-1)} \rangle}{\partial C^{(a,b)}} = \mathbb{1}_{0 \leq a \leq A} \delta_{a,b} \delta_{a,c-1} \frac{\partial \langle \phi^{(a)} \phi^{(a)} \rangle}{\partial C^{(a,a)}}.$$

Thus, we arrive at

$$\begin{aligned} \frac{\partial^2 \mathcal{S}_{\text{aux}}}{\partial C^{(a,b)} \partial \tilde{C}^{(c,d)}} &= -n \nu_{a-1} \delta_{(a,b),(c,d)} \\ &\quad + n \mathbb{1}_{0 \leq a \leq A} \delta_{a,b} \delta_{c,d} \delta_{a,c-1} \nu_{c-1} F_{c-1}, \\ F_{c-1} &:= g_c^2 \frac{\partial \langle \phi^{(c-1)} \phi^{(c-1)} \rangle}{\partial C^{(c-1,c-1)}}. \end{aligned} \quad (59)$$

Analogously, the other off-diagonal element is

$$\begin{aligned} \frac{\partial^2 \mathcal{S}_{\text{aux}}}{\partial \tilde{C}^{(a,b)} \partial C^{(c,d)}} &= -n \nu_{a-1} \delta_{(a,b),(c,d)} \\ &\quad + n \mathbb{1}_{0 \leq c \leq A} \delta_{a,b} \delta_{c,d} \delta_{c,a-1} \nu_{a-1} F_{a-1}. \end{aligned} \quad (60)$$

Finally, the diagonal element is

$$\begin{aligned} \frac{\partial^2 \mathcal{S}_{\text{aux}}}{\partial \tilde{C}^{(a,b)} \partial \tilde{C}^{(c,d)}} &= \mathbb{1}_{a \geq 1} \delta_{a,b} \delta_{a,c} \delta_{c,d} n \nu_{a-1} G_{a-1} \\ G_{a-1} &:= g_a^4 \langle \phi^{(a-1)} \phi^{(a-1)} \phi^{(a-1)} \phi^{(a-1)} \rangle \\ &\quad - g_a^4 \langle \phi^{(a-1)} \phi^{(a-1)} \rangle^2. \end{aligned}$$

With the Hessian at hand, we proceed to the propagator, i.e., the inverse of the Hessian $-\sum_k \sum_{c,d} \mathcal{S}_{\text{aux},ik}^{(a,b),(c,d)} \Delta_{kj}^{(c,d),(e,f)} = \delta_{(a,b),(e,f)} \delta_{i,j}$.

Due to the structure of the Hessian (58), the propagator has the structure

$$\Delta = \begin{pmatrix} \Delta_{11} & \Delta_{12} \\ \Delta_{21} & 0 \end{pmatrix}.$$

We first consider the off-diagonal elements Δ_{12} , which are time-reversed functions of one another $\Delta_{12}^{(a,b),(c,d)} = \Delta_{21}^{(c,d),(a,b)}$, and can be determined from $-\mathcal{S}_{\text{aux},21}\Delta_{12} = \mathbf{1}$ or, more explicitly,

$$-\sum_{c,d} \frac{\partial^2 \mathcal{S}_{\text{aux}}}{\partial \tilde{C}^{(a,b)} \partial C^{(c,d)}} \Delta_{12}^{(c,d),(e,f)} = \delta_{(a,b),(e,f)}.$$

Using the explicit expression (60) we obtain the Dyson equation

$$\begin{aligned} \nu_{a-1} n \Delta_{12}^{(a,b),(e,f)} - n \mathbb{1}_{1 \leq a \leq A+1} \delta_{a,b} \nu_{a-1} F_{a-1} \Delta_{12}^{(a-1,a-1),(e,f)} \\ = \delta_{(a,b),(e,f)}. \end{aligned}$$

From here, we implicitly assume $1 \leq a \leq A+1$ and drop the indicator $\mathbb{1}_{1 \leq a \leq A+1}$. Evaluating this equation for $a \neq b$ we get

$$\Delta_{12}^{(a,b),(e,f)} = (\nu_{a-1} n)^{-1} \delta_{(a,b),(e,f)} \quad \text{for } a \neq b. \quad (61)$$

For $a = b$ one obtains an iterative equation

$$\nu_{a-1} n \Delta_{12}^{(a,a),(e,f)} - n \nu_{a-1} F_{a-1} \Delta_{12}^{(a-1,a-1),(e,f)} = \delta_{(a,a),(e,f)}.$$

Due to linearity, a valid solution for $e \neq f$ is $\Delta_{12} \equiv 0$. For $e = f$ we obtain the single-index iteration

$$\Delta_{12}^{(a,a),(e,e)} = (\nu_{a-1} n)^{-1} \delta_{(a,a),(e,e)} + F_{a-1} \Delta_{12}^{(a-1,a-1),(e,e)}, \quad (62)$$

with the initial condition

$$\Delta_{12}^{(a,a),(a,a)} = (\nu_{a-1} n)^{-1}$$

and for $a > e$ obeying the iteration

$$\Delta_{12}^{(a,a),(e,e)} = F_{a-1} \Delta_{12}^{(a-1,a-1),(e,e)}$$

which has the solution

$$\Delta_{12}^{(a,a),(e,e)} = \mathbb{1}_{a \geq e} n^{-1} \nu_{e-1}^{-1} \prod_{k=e}^{a-1} F_k \quad (63)$$

with $\prod_{k=e}^{e-1} F_k \equiv 1$. Finally, we need to determine Δ_{11} which obeys

$$\begin{aligned} -\sum_{c,d} \mathcal{S}_{\text{aux},21}^{(a,b),(c,d)} \Delta_{11}^{(c,d),(e,f)} - \sum_{c,d} \mathcal{S}_{\text{aux},22}^{(a,b),(c,d)} \Delta_{21}^{(c,d),(e,f)} &= 0, \\ -\sum_{c,d} \mathcal{S}_{\text{aux},11}^{(a,b),(c,d)} \Delta_{11}^{(c,d),(e,f)} - \sum_{c,d} \mathcal{S}_{\text{aux},12}^{(a,b),(c,d)} \Delta_{21}^{(c,d),(e,f)} &= \delta_{(a,b),(e,f)}. \end{aligned}$$

Since $\mathcal{S}_{\text{aux},11} \equiv 0$, the second equation is fulfilled by the solution of Δ_{21} alone. The first equation yields an additional condition for Δ_{11} , which we obtain by using $-\mathcal{S}_{\text{aux},21} = \Delta_{12}^{-1}$. Thus, multiplying from left with Δ_{12} yields

$$\Delta_{11} = \Delta_{12} \mathcal{S}_{\text{aux},22} \Delta_{21}. \quad (64)$$

Written explicitly, this results in

$$\begin{aligned} \Delta_{11}^{(a,b),(c,d)} &= \sum_{(a',b'),(c',d')} \Delta_{12}^{(a,b),(a',b')} \mathcal{S}_{\text{aux},22}^{(a',b'),(c',d')} \Delta_{21}^{(c',d'),(c,d)} \\ &= \sum_{a'} \Delta_{12}^{(a,b),(a',a')} \left[n \nu_{a'-1} G_{a'-1} \right] \Delta_{21}^{(a',a'),(c,d)}. \end{aligned}$$

Only entries Δ_{12} with equal indices in the second pair appear which fulfill the iteration Eq. (62). In addition, we have that $\Delta_{12}^{(a \neq b), (a', a')} \equiv 0$ due to Eq. (61). Thus, we arrive at

$$\Delta_{11}^{(a,b),(c,d)} = n^{-1} \delta_{a,b} \delta_{c,d} \sum_{a'=1}^{\min(a,d)} \left\{ \prod_{k=a'}^{a-1} F_k \right\} \nu_{a'-1}^{-1} G_{a'-1} \left\{ \prod_{l=a'}^{d-1} F_l \right\} \quad (65)$$

For $a = b = c = d$, this simplifies to

$$\Delta_{11}^{(a,a),(a,a)} = n^{-1} \sum_{a'=1}^a \left\{ \prod_{k=a'}^{a-1} F_k^2 \right\} \nu_{a'-1}^{-1} G_{a'-1}.$$

To determine the solution, we need to evaluate F_a and G_a .

For the ReLU activation function, we get from Eq. (57) the simple relation $\langle \phi^{(a)} \phi^{(a)} \rangle = \frac{1}{2} C^{(a,a)}$ and thus

$$F_{a-1} = \frac{1}{2} g_a^2. \quad (66)$$

For G_a we also need $\langle \phi^{(a)} \phi^{(a)} \phi^{(a)} \phi^{(a)} \rangle = \frac{3}{2} C^{(a,a)} C^{(a,a)}$, which follows from Wick's theorem, to obtain

$$G_{a-1} = \frac{5}{4} g_a^4 C^{(a-1,a-1)} C^{(a-1,a-1)}. \quad (67)$$

6.5.2. RNN The only difference between $\mathcal{W}_{\text{aux}}^{\text{DNN}}$ and $\mathcal{W}_{\text{aux}}^{\text{RNN}}$ is that the latter does not decompose into a sum, so the different time-points are not independent. The elements of the Hessian (58) therefore take the form

$$\frac{\partial^2 \mathcal{S}_{\text{aux}}}{\partial C^{(a,b)} \partial \tilde{C}^{(c,d)}} = -n \delta_{(a,b),(c,d)} + n g^2 \frac{\partial \langle \phi^{(c-1)} \phi^{(d-1)} \rangle}{\partial C^{(a,b)}}.$$

The derivative in the second term is the linear response of the expectation value $\langle \phi^{(c-1)} \phi^{(d-1)} \rangle$ with regard to changes of $C^{(a,b)}$. Since the former only depends on the joint statistics of $h^{(c-1)}, h^{(d-1)}$ and thus on $C^{(c-1,c-1)}, C^{(c-1,d-1)}$, and $C^{(d-1,d-1)}$ the matrix elements of $\partial^2 \mathcal{S}_{\text{aux}} / \partial C^{(a,b)} \partial \tilde{C}^{(c,d)}$ are only non-zero in a 2×2 block where at most two different indices appear in total. Analogously, the second term in

$$\frac{\partial^2 \mathcal{S}_{\text{aux}}}{\partial \tilde{C}^{(a,b)} \partial C^{(c,d)}} = -n \delta_{(a,b),(c,d)} + n g^2 \frac{\partial \langle \phi^{(a-1)} \phi^{(b-1)} \rangle}{\partial C^{(c,d)}}$$

depends only on $C^{(a-1,a-1)}, C^{(a-1,b-1)}$, and $C^{(b-1,b-1)}$ which leads again to a 2×2 block structure. The diagonal element is

$$\begin{aligned} \frac{\partial^2 \mathcal{S}_{\text{aux}}}{\partial \tilde{C}^{(a,b)} \partial \tilde{C}^{(c,d)}} &= n g^4 \langle \phi^{(a-1)} \phi^{(b-1)} \phi^{(c-1)} \phi^{(d-1)} \rangle \\ &\quad - n g^4 \langle \phi^{(a-1)} \phi^{(b-1)} \rangle \langle \phi^{(c-1)} \phi^{(d-1)} \rangle \\ &=: n G_{a-1,b-1,c-1,d-1}, \end{aligned}$$

which does not vanish for any combination of parameters.

The resulting propagator again obeys

$$-\sum_{c,d} \frac{\partial^2 \mathcal{S}_{\text{aux}}}{\partial \tilde{C}^{(a,b)} \partial C^{(c,d)}} \Delta_{12}^{(c,d),(e,f)} = \delta_{(a,b),(e,f)},$$

which explicitly reads

$$n \Delta_{12}^{(a,b),(e,f)} = \delta_{(a,b),(e,f)} + n g^2 \sum_{c,d} \frac{\partial \langle \phi^{(a-1)} \phi^{(b-1)} \rangle}{\partial C^{(c,d)}} \Delta_{12}^{(c,d),(e,f)}.$$

We restrict ourselves to $a = b = c = d$, i.e., $\Delta_{11}^{(a,a),(a,a)}$, for which it is by Eq. (64) sufficient to determine $\Delta_{12}^{(a,a),(e,f)}$. For $a = b$, we obtain

$$n \Delta_{12}^{(a,a),(e,f)} = \delta_{(a,a),(e,f)} + n \mathbb{1}_{1 \leq a \leq A+1} F_{a-1} \Delta_{12}^{(a-1,a-1),(e,f)}$$

because $g^2 \partial \langle \phi^{(a-1)} \phi^{(a-1)} \rangle / \partial C^{(d,c)} = g^2 \delta_{a-1,c} \delta_{a-1,d} F_{a-1}$. Thus, for $e = f$, we recovered Eq. (62) which is solved by Eq. (63). For $e \neq f$, $\Delta_{12}^{(a,a),(e,f)} \equiv 0$ due to the vanishing inhomogeneity.

The same expression (64) holds as in the case of the DNN,

$$\Delta_{11}^{(a,b),(c,d)} = \sum_{(a',b'),(c',d')} \Delta_{12}^{(a,b),(a',b')} \mathcal{S}_{\text{aux},22}^{(a',b'),(c',d')} \Delta_{21}^{(c',d'),(c,d)}.$$

For $\Delta_{11}^{(a,a),(a,a)}$ we obtain

$$\Delta_{11}^{(a,a),(a,a)} = n^{-1} \sum_{a',c'=1}^a \left\{ \prod_{k=a'}^{a-1} F_k \right\} G_{a'-1,a'-1,c'-1,c'-1} \left\{ \prod_{l=c'}^{a-1} F_l \right\} \quad (68)$$

because $\Delta_{12}^{(a,a),(e,f)} = 0$.

For the ReLU activation function, we need [51]

$$\begin{aligned} \langle \phi^{(a)} \phi^{(a)} \phi^{(b)} \phi^{(b)} \rangle &= \frac{3}{2\pi} \nu_{a,b}^2 \sin \theta_{a,b} \cos \theta_{a,b} \\ &+ \frac{1}{2\pi} \nu_{a,b}^2 (\pi - \theta_{a,b}) (1 + 2 \cos^2 \theta_{a,b}) \end{aligned} \quad (69)$$

with $\nu_{a,b} = \sqrt{C^{(a,a)} C^{(b,b)}}$ and $\theta_{a,b} = \cos^{-1} \left(\frac{C^{(a,b)}}{\nu_{a,b}} \right)$ as in Eq. (55). With this, we can determine

$$\begin{aligned} G_{a-1,a-1,c-1,c-1} &= g^4 \langle \phi^{(a-1)} \phi^{(a-1)} \phi^{(c-1)} \phi^{(c-1)} \rangle \\ &- \frac{1}{4} g^4 C^{(a-1,a-1)} C^{(c-1,c-1)}. \end{aligned}$$

References

- [1] Hinton G E, Osindero S and Teh Y W 2006 *Neural Comput.* **18** 1527–1554
- [2] Krizhevsky A, Sutskever I and Hinton G E 2012 *Adv. Neural Inf. Process. Syst.* vol 25 ed Pereira F, Burges C J C, Bottou L and Weinberger K Q (Curran Associates, Inc.) pp 1097–1105 URL <https://proceedings.neurips.cc/paper/2012/file/c399862d3b9d6b76c8436e924a68c45b-Paper.pdf>
- [3] Hannun A, Case C, Casper J, Catanzaro B, Diamos G, Elsen E, Prenger R, Satheesh S, Sengupta S, Coates A *et al.* 2014 *ArXiv*
- [4] LeCun Y, Bengio Y and Hinton G 2015 *Nature* **521** 436–444
- [5] Szegedy C, Zaremba W, Sutskever I, Bruna J, Erhan D, Goodfellow I and Fergus R 2014 *International Conference on Learning Representations* URL <http://arxiv.org/abs/1312.6199>

- [6] Neal R M 1996 *Bayesian Learning for Neural Networks* (Springer New York) URL <https://doi.org/10.1007/978-1-4612-0745-0>
- [7] Williams C 1996 *Adv. Neural Inf. Process. Syst.* vol 9 ed Mozer M, Jordan M and Petsche T (MIT Press) URL <https://proceedings.neurips.cc/paper/1996/file/ae5e3ce40e0404a45ecacaaf05e5f735-Paper.pdf>
- [8] Lee J, Sohl-Dickstein J, Pennington J, Novak R, Schoenholz S and Bahri Y 2018 *International Conference on Learning Representations* URL <https://openreview.net/forum?id=B1EA-M-OZ>
- [9] Matthews A G d G, Hron J, Rowland M, Turner R E and Ghahramani Z 2018 *International Conference on Learning Representations* URL <https://openreview.net/forum?id=H1-nGgWC->
- [10] Jacot A, Gabriel F and Hongler C 2018 *Advances in Neural Information Processing Systems 31* pp 8580–8589 URL <https://proceedings.neurips.cc/paper/2018/file/5a4be1fa34e62bb8a6ec6b91d2462f5a-Paper.pdf>
- [11] Lee J, Schoenholz S, Pennington J, Adlam B, Xiao L, Novak R and Sohl-Dickstein J 2020 *Adv. Neural Inf. Process. Syst.* vol 33 ed Larochelle H, Ranzato M, Hadsell R, Balcan M and Lin H (Curran Associates, Inc.) pp 15156–15172 URL <https://proceedings.neurips.cc/paper/2020/file/ad086f59924ffffe0773f8d0ca22ea712-Paper.pdf>
- [12] Rumelhart David E, Hinton Geoffrey E and Williams Ronald J 1986 *Nature* **323** 533–536 URL <https://doi.org/10.1038/323533a0>
- [13] Pearlmutter B A 1989 *Neural Comput.* **1** 263–269
- [14] Yang G 2019 *Adv. Neural Inf. Process. Syst.* vol 32 ed Wallach H, Larochelle H, Beygelzimer A, d'Alché-Buc F, Fox E and Garnett R (Curran Associates, Inc.) URL <https://proceedings.neurips.cc/paper/2019/file/5e69fda38cda2060819766569fd93aa5-Paper.pdf>
- [15] Alemohammad S, Wang Z, Balestrieri R and Baraniuk R 2021 *International Conference on Learning Representations* URL <https://openreview.net/forum?id=3T9iFICe0Y9>
- [16] Alemohammad S, Balestrieri R, Wang Z and Baraniuk R 2020 URL <https://arxiv.org/abs/2012.04859>
- [17] Yaida S 2020 *Proceedings of The First Mathematical and Scientific Machine Learning Conference (Proceedings of Machine Learning Research* vol 107) ed Lu J and Ward R (Princeton University, Princeton, NJ, USA: PMLR) pp 165–192 URL <http://proceedings.mlr.press/v107/yaida20a.html>
- [18] Dyer E and Gur-Ari G 2020 *International Conference on Learning Representations* URL <https://openreview.net/forum?id=S1gFvANKDS>
- [19] Antognini J M 2019 *ArXiv*
- [20] Huang J and Yau H T 2020 *International Conference on Machine Learning* (PMLR) pp 4542–4551
- [21] Aitken K and Gur-Ari G 2020 URL <https://arxiv.org/abs/2006.06687>
- [22] Halverson J, Maiti A and Stoner K 2021 *Machine Learning: Science and Technology* **2** 035002 URL <https://doi.org/10.1088/2632-2153/abeca3>
- [23] Naveh G, Ben David O, Sompolinsky H and Ringel Z 2021 *Phys. Rev. E* **104**(6) 064301 URL <https://link.aps.org/doi/10.1103/PhysRevE.104.064301>

- [24] Zavatore-Veth J A, Canatar A, Ruben B and Pehlevan C 2021 *Adv. Neural Inf. Process. Syst.* ed Beygelzimer A, Dauphin Y, Liang P and Vaughan J W URL <https://openreview.net/forum?id=1oRFmD0F1-5>
- [25] Naveh G and Ringel Z 2021 *Adv. Neural Inf. Process. Syst.* ed Beygelzimer A, Dauphin Y, Liang P and Vaughan J W URL <https://openreview.net/forum?id=vBYwwBxVcsE>
- [26] Zavatore-Veth J A and Pehlevan C 2021 *Adv. Neural Inf. Process. Syst.* ed Beygelzimer A, Dauphin Y, Liang P and Vaughan J W URL <https://openreview.net/forum?id=MxE7xFzv0N8>
- [27] Noci L, Bachmann G, Roth K, Nowozin S and Hofmann T 2021 *Adv. Neural Inf. Process. Syst.* ed Beygelzimer A, Dauphin Y, Liang P and Vaughan J W URL <https://openreview.net/forum?id=DTA7Bgrai-Q>
- [28] Roberts D A, Yaida S and Hanin B 2022 *The Principles of Deep Learning Theory* (Cambridge University Press) URL <https://doi.org/10.1017/9781009023405>
- [29] Grosvenor K T and Jefferson R 2022 *SciPost Phys.* **12**(3) 81 URL <https://scipost.org/10.21468/SciPostPhys.12.3.081>
- [30] Williams C K and Rasmussen C E 2006 *Gaussian Processes for Machine Learning* 1st ed (Cambridge: MIT Press)
- [31] Sompolinsky H, Crisanti A and Sommers H J 1988 *Phys. Rev. Lett.* **61**(3) 259–262 URL <http://link.aps.org/doi/10.1103/PhysRevLett.61.259>
- [32] Chow C and Buice M 2015 *J. Math. Neurosci.* **5** 8
- [33] Hertz J A, Roudi Y and Sollich P 2017 *J. Phys. A* **50** 033001 URL <http://stacks.iop.org/1751-8121/50/i=3/a=033001>
- [34] Martí D, Brunel N and Ostojic S 2018 *Phys. Rev. E* **97**(6) 062314 URL <https://link.aps.org/doi/10.1103/PhysRevE.97.062314>
- [35] Crisanti A and Sompolinsky H 2018 *Phys. Rev. E* **98**(6) 062120 URL <https://link.aps.org/doi/10.1103/PhysRevE.98.062120>
- [36] Schuecker J, Goedeke S and Helias M 2018 *Phys. Rev. X* **8**(4) 041029 URL <https://link.aps.org/doi/10.1103/PhysRevX.8.041029>
- [37] Parisi G 1980 *J. Phys. A Math. Gen.* **13** 1101
- [38] Sommers H 1987 *Phys. Rev. Lett.* **58** 1268–1271
- [39] Fischer K and Hertz J 1991 *Spin glasses* (Cambridge University Press)
- [40] Mozeika A, Li B and Saad D 2020 *Phys. Rev. Lett.* **125**(16) 168301 URL <https://link.aps.org/doi/10.1103/PhysRevLett.125.168301>
- [41] Molgedey L, Schuchhardt J and Schuster H 1992 *Phys. Rev. Lett.* **69** 3717
- [42] Schuecker J, Goedeke S, Dahmen D and Helias M 2016 *ArXiv* 1605.06758 [cond-mat.dis-nn]
- [43] Zinn-Justin J 1996 *Quantum field theory and critical phenomena* (Clarendon Press, Oxford)
- [44] Moshe M and Zinn-Justin J 2003 *Phys. Rep.* **385** 69–228 ISSN 0370-1573 URL <http://www.sciencedirect.com/science/article/pii/S0370157303002631>
- [45] MacKay D J 2003 *Information theory, inference and learning algorithms* (Cambridge university press)

- [46] Hertz J, Krogh A and Palmer R G 1991 *Introduction to the Theory of Neural Computation* (Perseus Books) ISBN 0-201-51560-1
- [47] Sompolinsky H and Zippelius A 1981 *Phys. Rev. Lett.* **47**(5) 359–362 URL <http://link.aps.org/doi/10.1103/PhysRevLett.47.359>
- [48] Helias M and Dahmen D 2020 *Statistical Field Theory for Neural Networks* (Springer International Publishing)
- [49] Coolen A 2001 *Neuro-Informatics and Neural Modelling (Handbook of Biological Physics* vol 4) ed Moss F and Gielen S (North-Holland) pp 619–684
- [50] Gretton A, Borgwardt K M, Rasch M J, Schölkopf B and Smola A 2012 *J. Mach. Learn. Res.* **13** 723–773 URL <http://jmlr.org/papers/v13/gretton12a.html>
- [51] Cho Y and Saul L 2009 *Adv. Neural Inf. Process. Syst.* vol 22 ed Bengio Y, Schuurmans D, Lafferty J, Williams C and Culotta A (Curran Associates, Inc.) URL <https://proceedings.neurips.cc/paper/2009/file/5751ec3e9a4feab575962e78e006250d-Paper.pdf>
- [52] Chen M, Pennington J and Schoenholz S 2018 *Proceedings of the 35th International Conference on Machine Learning (Proceedings of Machine Learning Research* vol 80) ed Dy J and Krause A (PMLR) pp 873–882 URL <http://proceedings.mlr.press/v80/chen18i.html>
- [53] Hron J, Bahri Y, Novak R, Pennington J and Sohl-Dickstein J 2020 URL <https://arxiv.org/abs/2006.10541>
- [54] van Meegen A, Kühn T and Helias M 2021 *Phys. Rev. Lett.* **127**(15) 158302 URL <https://link.aps.org/doi/10.1103/PhysRevLett.127.158302>
- [55] Harris C R, Millman K J, van der Walt S J, Gommers R, Virtanen P, Cournapeau D, Wieser E, Taylor J, Berg S, Smith N J, Kern R, Picus M, Hoyer S, van Kerkwijk M H, Brett M, Haldane A, Fernández del Río J, Wiebe M, Peterson P, Gérard-Marchant P, Sheppard K, Reddy T, Weckesser W, Abbasi H, Gohlke C and Oliphant T E 2020 *Nature* **585** 357–362
- [56] Virtanen P, Gommers R, Oliphant T E, Haberland M, Reddy T, Cournapeau D, Burovski E, Peterson P, Weckesser W, Bright J, van der Walt S J, Brett M, Wilson J, Millman K J, Mayorov N, Nelson A R J, Jones E, Kern R, Larson E, Carey C J, Polat İ, Feng Y, Moore E W, VanderPlas J, Laxalde D, Perktold J, Cimrman R, Henriksen I, Quintero E A, Harris C R, Archibald A M, Ribeiro A H, Pedregosa F, van Mulbregt P and SciPy 10 Contributors 2020 *Nat. Methods* **17** 261–272
- [57] Williams C K 1998 *Neural Comput.* **10** 1203–1216
- [58] van Meegen A and van Albada S J 2021 *Phys. Rev. Res.* **3**(4) 043077 URL <https://link.aps.org/doi/10.1103/PhysRevResearch.3.043077>